https://doi.org/10.5194/egusphere-2026-4418
Preprint. Discussion started: 30 July 2026
© Author(s) 2026. CC BY 4.0 License.

Agricultural flood risk under seasonally varying rainfall extremes and crop vulnerability

Antonio Annis[1,2,3,4], Fernando Nardi[5], and Marco Marani[1,2]

[1]Department of Civil, Environmental and Architectural Engineering, University of Padua
[2]Research Center on Climate Change Impacts, University of Padova - Rovigo Campus
[3]Department of Geosciences, University of Padova
[4]Department of Land, Environment, Agriculture and Forestry, University of Padova
[5]Department of Civil Engineering and Computer Science Engineering, Tor Vergata University

Correspondence: Antonio Annis (antonio.annis@unipd.it)

Abstract. Agricultural systems are highly vulnerable to flooding, particularly when extreme precipitation events occur during sensitive crop growth stages. However, most flood-risk assessments rely on static annual hazard scenarios and simplified design storms, neglecting the combined effects of hydrological seasonality, rainfall temporal structure, and crop phenology. In this study, we propose a probabilistic-hydrological-hydraulic framework for agricultural flood-risk assessment under seasonally varying short-duration extreme precipitation. The approach integrates non-asymptotic multivariate frequency analysis, copula-based dependence modelling among rainfall durations, stochastic microcanonical rainfall disaggregation, hydraulic simulations, and crop-specific flood depth-duration vulnerability functions. Flood-hazard maps are generated at the monthly scale and coupled with seasonally varying crop exposure and vulnerability conditions. The framework is applied to a flood-prone agricultural area in northern Italy. Results show that rainfall temporal structure and event duration substantially influence expected annual losses, with long-duration events generally producing the highest damages due to prolonged inundation and waterlogging conditions. The copula-based multi-duration analysis reveals a considerable uncertainty associated with inter-duration dependence, highlighting that the use of a single representative storm duration may significantly bias agricultural flood-risk estimates. The adopted microcanonical rainfall generator also proved effective in reproducing realistic multi-burst rainfall structures and temporally clustered events, which are particularly relevant for representing cumulative soil saturation and flood persistence processes. Overall, the proposed methodology provides a physically consistent and transferable framework for probabilistic agricultural flood-risk assessment and may support climate-risk analyses, adaptation planning, and flood-risk management in agricultural systems exposed to increasingly complex hydrometeorological extremes.

1 Introduction

In flood risk assessment, vulnerability is most often treated as a fixed property of the exposed asset: a building damaged by a given inundation depth is assumed to suffer the same loss whichever day of the year the flood occurs. Agricultural systems violate this assumption. A crop's response to flooding depends on its phenological stage, so that the same event may cause negligible or near-total loss depending on whether it strikes at sowing, vegetative growth, flowering, or harvest (Scorzini et al.,

https://doi.org/10.5194/egusphere-2026-4418
Preprint. Discussion started: 30 July 2026
© Author(s) 2026. CC BY 4.0 License.

2026; Lucaora et al., 2025). Vulnerability in cultivated floodplains is therefore not a static curve but a moving target that tracks the crop calendar. This temporal dimension matters precisely where it is most often ignored. Flood risk methods have matured around urban and infrastructural exposure, while agricultural areas — highly exposed in the floodplain and increasingly enlisted to accommodate excess water under modern floodplain-management strategies (Bremond et al., 2013) — remain comparatively under-served, despite their role in food production and rural economies. This temporal dependency is further emphasized in physically-based damage assessment studies, such as Lucaora et al. (2025), where crop losses are shown to vary significantly across months due to the interaction between flood characteristics and crop growth stages. Similarly, damage functions developed for agricultural systems explicitly account for growth stages as a primary control on losses (Shrestha et al., 2016, 2019, 2021). More broadly, comprehensive reviews of agricultural flood damage modelling highlight that seasonality is a key driver of crop losses, although it is often represented through simplified calendar-based schemes (Bremond et al., 2013). In addition to phenological sensitivity, flood impacts on crops are strongly influenced by inundation, and persistence. Prolonged soil saturation can induce hypoxic conditions in the root zone, leading to root asphyxia, reduced nutrient uptake, and, in severe cases, plant mortality. These processes make agricultural damage particularly sensitive to the temporal dynamics of flooding, rather than to peak water levels alone. Consequently, a realistic assessment of agricultural flood risk requires an accurate representation of both flood timing and flood duration, as well as their interaction with crop development stages (Bremond et al., 2013).

Nonetheless, most existing flood risk assessments rely on hazard representations based on annual exceedance probabilities derived from deterministic flood maps. By assigning annual exceedance probabilities without resolving the timing of flood occurrence within the year, these scenarios cannot represent the alignment between seasonal flood hazard and crop vulnerability and therefore ignore the fact that a flood of given severity produces very different losses depending on when in the growing season it occurs. This assumption is poorly suited for agricultural applications: as discussed by Scorzini et al. (2021), annual hazard representations cannot resolve the intra-annual variability of flood occurrence and its alignment with crop vulnerability, potentially biasing damage estimates. To address this issue, recent studies have introduced seasonal components into risk assessment, for instance by estimating monthly flood probabilities and combining them with time-dependent vulnerability functions (Scorzini et al., 2026). Nevertheless, even in these advanced approaches, a fundamental limitation remains: seasonality is typically incorporated only on the vulnerability side, while flood hazard is still represented by a fixed set of maps associated with return periods that do not vary with seasons within the year. For example, Lucaora et al. (2025) combined high-resolution 1D–2D hydraulic modelling with crop-specific vulnerability functions to estimate spatially distributed agricultural damage, explicitly accounting for monthly variability in crop sensitivity. However, the flood hazard scenarios are derived from return-period-based forcing that remains unchanged across months, thereby neglecting the potential seasonal variability of flood-generating processes. This limitation is consistent with broader findings in the literature, which show that most agricultural damage models rely on simplified hazard representations and often consider only a subset of relevant flood characteristics (Bremond et al., 2013). This limitation is closely related to the representation of extreme precipitation used in hydrological and hydraulic models. Standard design storm approaches, such as Chicago or Euler-type storms, are commonly derived from intensity–duration–frequency (IDF) curves and assume that precipitation intensities across all durations corre-

https://doi.org/10.5194/egusphere-2026-4418
Preprint. Discussion started: 30 July 2026
© Author(s) 2026. CC BY 4.0 License.

spond to the same return period. However, recent work by Cache et al. (2025) has shown that this assumption is physically unrealistic, as precipitation intensities at different durations are statistically dependent and rarely share the same return period within a single event. By introducing a joint return period framework, based on multivariate dependence structures, Cache et al. (2025) demonstrate that traditional design storms can systematically overestimate total precipitation depths and misrepresent the temporal structure of extreme events.

These findings have important implications for flood hazard modelling, particularly for agricultural ecosystems. The temporal structure of precipitation events controls not only peak discharge but also flood volume, hydrograph shape, and recession dynamics, which in turn determine inundation duration and water persistence on fields. Moreover, the dominant precipitation-generating mechanisms vary seasonally: convective events typically produce short, high-intensity rainfall bursts, while stratiform systems generate longer-duration and more persistent precipitation. As a result, the relation between event rarity, duration, and temporal rainfall distribution is inherently seasonal, and cannot be adequately represented by a single, time-invariant design storm approach. From a damage modelling perspective, several methodologies have been developed to quantify flood impacts on agriculture. Early frameworks, such as those reviewed by Bremond et al. (2013), rely on empirical or synthetic damage functions relating crop losses to flood characteristics such as water depth, duration, and timing, often focusing primarily on direct crop damage. More recent approaches, including AGRIDE-c (Scorzini et al., 2021), extend these concepts by integrating multiple hazard variables and crop-specific parameters within a probabilistic risk framework. Physically based approaches, such as Lucaora et al. (2025), further advance the field by coupling hydrodynamic simulations with crop vulnerability dynamics, enabling spatially distributed estimates of damage at high resolution. Despite these advances, most models still rely on hazard representations that do not explicitly account for seasonal variability in precipitation structure and flood response.

These gaps highlight the need for an integrated framework that consistently represents the seasonal coupling between precipitation extremes, flood dynamics, and crop vulnerability. In particular, there is a need to account for the multivariate nature of short-duration precipitation extremes, propagate this variability through hydrological and hydraulic models to obtain season-specific flood hazard, and combine these hazard scenarios with seasonally varying crop vulnerability in a coherent risk assessment framework.

In this study, we address these challenges by proposing a novel probabilistic–hydrological–hydraulic framework for agricultural flood-risk assessment under seasonal short-duration extreme precipitation. The proposed approach builds upon recent advances in multivariate extreme value analysis and stochastic design storm generation (Cache et al., 2025), integrating them within a modelling chain that produces flood-hazard maps that explicitly vary at the monthly scale. These maps are then coupled with crop-specific vulnerability functions evolving throughout the growing season. The proposed framework specifically focuses on the cascading effects of rainfall-related uncertainty into agricultural flood-risk estimates, including uncertainty associated with multi-duration frequency analysis, inter-duration dependence, and rainfall temporal structure. The main contributions of this study are fourfold. First, we introduce a risk formulation that explicitly incorporates both hydrological seasonality and time-dependent crop vulnerability. Second, we develop a modelling chain generating seasonally consistent flood-hazard maps, moving beyond the use of static annual flood scenarios. Third, we integrate a non-asymptotic extreme-value approach within a multivariate framework to represent short-duration precipitation extremes and their dependencies across temporal

https://doi.org/10.5194/egusphere-2026-4418
Preprint. Discussion started: 30 July 2026
© Author(s) 2026. CC BY 4.0 License.

scales. Fourth, we explicitly account for the influence of rainfall temporal structure and event duration on flood persistence and crop damage through the integration of multi-duration hydraulic simulations and depth-duration vulnerability functions. By explicitly linking the timing, temporal organization, and dependence structure of extreme precipitation to flood dynamics and crop vulnerability, the proposed framework provides a physically consistent basis for probabilistic agricultural flood-risk assessment and supports the development of targeted adaptation strategies in flood-prone agricultural systems.

2 Methodology

A workflow of the proposed methodology is shown in Fig. 1. The expression of the expected crop annual loss, illustrated in Section 2.1 is the result of the combination of seasonally varying hazard (Section 2.2), vulnerability, and exposure (Section 2.3). Ensembles of monthly hazard maps generated through a hydrological-hydraulic model (Section 2.2.2) consider the uncertainties given by the dependencies across temporal scales of short-duration precipitation extremes with a copula-based approach (Section 2.2.1) and by the distribution of the rainfall peaks (i.e. the within-event temporal structure) with a micro-canonical model (Section 2.2.1). The framework is organized around three linked levels. The statistical level describes which rainfall events are plausible in each month and how rainfall accumulations at different durations co-vary within the same event. The hydrological–hydraulic level translates these synthetic events into spatially distributed flood depths and inundation durations. The impact level combines these hazard variables with the crop calendar, exposed area, yield, and depth–duration vulnerability functions. This structure allows rainfall seasonality and crop seasonality to enter the risk calculation simultaneously, rather than treating hazard as annual and vulnerability as seasonal.

https://doi.org/10.5194/egusphere-2026-4418
Preprint. Discussion started: 30 July 2026
© Author(s) 2026. CC BY 4.0 License.

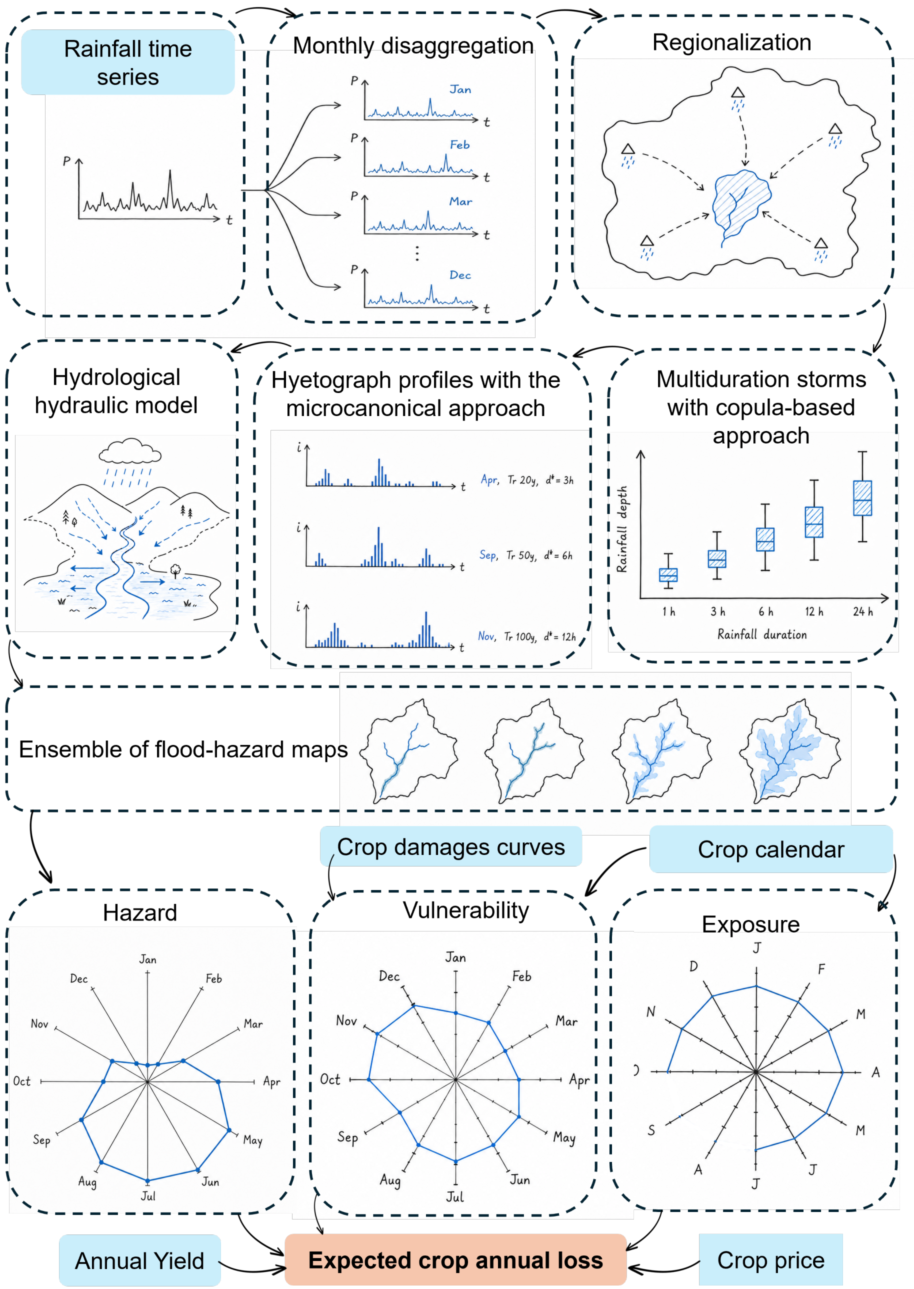

Figure 1. Flowchart of the proposed methodology for estimating expected annual crop loss. Light-blue boxes denote input data, dashed white boxes denote methodological steps, and the orange box denotes the final output.

https://doi.org/10.5194/egusphere-2026-4418
Preprint. Discussion started: 30 July 2026
© Author(s) 2026. CC BY 4.0 License.

2.1 Expected annual agricultural loss (EAL) formulation

The agricultural year is discretised into n monthly blocks, $m = 1, \ldots, n$, defined according to the crop calendar. For each monthly block m, flood hazard is represented by a severity variable that, in principle, is continuous and may be interpreted as a measure of flood intensity or magnitude relevant for agricultural damage, such as inundation depth, flood extent, inundation duration, flow magnitude, or a composite hazard metric. In practice, this continuous severity space is discretised into K non-overlapping classes, or bins, indexed by $i = 1, \ldots, K$.

The severity bins are defined by thresholds associated with the return-period scenarios T_i used in the hydraulic simulations. Each class i represents damaging flood events falling within a given return-period range, and is assigned the hydraulic response associated with the representative scenario T_i.

The random variable B_m denotes the flood severity class occurring in month-block m: $B_m = i$ if a damaging flood event belonging to severity class i occurs, and $B_m = 0$ if no damaging flood occurs in month-block m. Month blocks here coincide with calendar months. The probability associated with each severity class is denoted as

$$p_{m,i} = \mathbb{P}(B_m = i). \tag{1}$$

The probability that any damaging flood occurs in month m is therefore

$$p_m^{\text{tot}} = \mathbb{P}(B_m \neq 0) = \sum_{i=1}^{K} p_{m,i}. \tag{2}$$

For a given crop c, month m, and severity class i, the flood-induced production loss is a deterministic quantity obtained from the spatial damage model:

$$L_{m,i}^c = A_{m,c}\, y_c\, d_{c,m}(T_i), \tag{3}$$

where $L_{m,i}^c$ is the production loss (ton), $A_{m,c}$ the exposed area (ha), y_c the crop yield (ton ha^{-1}), and $d_{c,m}(T_i)$ the dimensionless damage fraction associated with the inundation depth and duration produced by the hydraulic simulation for return period T_i. Note that production losses can be expressed in monetary terms by multiplying $L_{m,i}^c$ by the crop price per unit production.

The expected loss within a single monthly block, obtained by considering all severity classes, is

$$\text{EL}_m^c = \sum_{i=1}^{K} p_{m,i}\, L_{m,i}^c. \tag{4}$$

This quantity represents the standalone expected production loss in month m, before accounting for the possibility that the crop may already have been damaged by a previous flood within the same growing season. Agricultural flood damage is characterised by strong temporal dependence: once a damaging flood occurs, the crop may be partially or completely compromised, and subsequent flood events within the same growing season cannot be treated as having fully additive impacts. To account for this effect, a first-hit assumption is adopted and illustrated as follows. We define the survival event S_m as the condition that no damaging flood has occurred in any of the preceding months:

$$S_m = \bigcap_{k=1}^{m-1} \{B_k = 0\}. \tag{5}$$

https://doi.org/10.5194/egusphere-2026-4418
Preprint. Discussion started: 30 July 2026
© Author(s) 2026. CC BY 4.0 License.

Under the first-hit assumption, the loss in month m contributes to the annual loss at its full value only if no damaging flood has occurred earlier in the season (i.e., if S_m holds). This does not mean that a crop already affected by an earlier flood would suffer no further physical damage from a subsequent event. Rather, it reflects the modelling choice of avoiding the unrealistic full accumulation of multiple crop losses after the crop has already been substantially damaged or destroyed by a previous event, a simplification whose implications are discussed in Section 5. Assuming statistical independence of flood occurrence between different months, the probability of survival up to month m is

$$\mathbb{P}(S_m) = \prod_{k=1}^{m-1} \mathbb{P}(B_k = 0) = \prod_{k=1}^{m-1} \left(1 - p_k^{\text{tot}}\right), \tag{6}$$

where $p_k^{\text{tot}} = \sum_{i=1}^{K} p_{k,i}$.

The corresponding indicator function is defined as

$$\mathbb{I}_{S_m} = \begin{cases} 1, & \text{if } S_m \text{ occurs,} \\ 0, & \text{otherwise.} \end{cases} \tag{7}$$

Conditional on this survival state, the random loss in month m remains severity-dependent and can be written as

$$L_m^c = \begin{cases} L_{m,i}^c, & \text{if } B_m = i, \quad i = 1, \ldots, K, \\ 0, & \text{if } B_m = 0. \end{cases} \tag{8}$$

Thus, flood severity affects both the probability of occurrence, through $p_{m,i}$, and the magnitude of the loss, through $L_{m,i}^c$. This distinction is important because different return-period scenarios generate different inundation depths and durations, and therefore different crop damage fractions. The expected contribution of month m is therefore

$$\mathbb{E}[\mathbb{I}_{S_m} L_m^c] = \mathbb{P}(S_m) \sum_{i=1}^{K} p_{m,i} L_{m,i}^c, \tag{9}$$

where the equality assumes that, conditional on the crop calendar, flood occurrence and severity in month m are independent of damaging events in previous months. The term in the summation corresponds to the standalone monthly expected loss, whereas $\mathbb{P}(S_m)$ downweights this loss by the probability that the crop has not already been affected by a previous damaging flood.

Substituting the survival probability into the monthly expected contribution yields the expected annual loss for crop c:

$$\text{EAL}^c = \sum_{m=1}^{n} \sum_{i=1}^{K} \left[\prod_{k=1}^{m-1} \left(1 - p_k^{\text{tot}}\right) \right] p_{m,i} L_{m,i}^c. \tag{10}$$

This expression represents the expected annual agricultural loss accounting for intra-annual timing of events and non-additive crop damage dynamics.

https://doi.org/10.5194/egusphere-2026-4418
Preprint. Discussion started: 30 July 2026
© Author(s) 2026. CC BY 4.0 License.

2.2 Hazard model

2.2.1 Statistical framework for the synthetic hyetograph generation

Traditional design–storm approaches typically rely on a single synthetic event associated with a prescribed return period and duration. However, precipitation processes are intrinsically stochastic and characterized by substantial variability in both the co-occurrence of intensities across temporal scales and in the estimation of extreme statistics. As a consequence, representing rainfall hazard through a single deterministic hyetograph may lead to biased crop-risk estimates, since impacts depend not only on the severity of rainfall at a given duration but also on the temporal structure of precipitation and the possible concurrence of multiple rainfall accumulations within the same event.

To address this limitation, we adopt a stochastic storm generator based on the concept of joint return-period proposed by Cache et al. (2025), in which rainfall depths across multiple durations are simulated consistently with the observed duration–frequency dependence structure. Here, however, the framework is extended to explicitly propagate uncertainty into the impact assessment. Instead of generating a single ensemble conditioned on a fixed duration–depth pair, we generate multiple ensembles anchored to different durations and return periods. Furthermore, rainfall statistics are estimated separately for each month to account for seasonally varying precipitation regimes, and a bootstrap resampling of events exceeding a given return period is applied to represent sampling uncertainty in extreme-value estimation.

This strategy allows us to represent two complementary sources of variability, besides the seasonal one: statistical uncertainty in the estimation and sampling of synthetic rainfall, and physical variability arising from the possible coexistence of different critical durations within a storm. The resulting ensemble of precipitation time series therefore provides a probabilistic characterization of rainfall forcing, enabling crop-risk evaluation to account for both rainfall generation uncertainty and intra-event temporal variability, while considering how hazard changes with the change of the phenological stages of the crops.

Seasonal disaggregation

Rain gage time series were first disaggregated at a monthly scale, and rainfall events were identified as independent storms separated by a 24-hour dry hiatus, following Marra et al. (2020). Because the interest is here in events that induce non-zero crop damage, i.e. extreme rainfall events with return periods longer than 1 year, it is useful to adopt an extreme value approach. Since the starting point are "ordinary events", it is advantageous to adopt an extreme value distribution that is directly connected to the ordinary event distribution and accounts for the number of events that may occur within a month. This requires moving away from traditional extreme-value theory, which is an asymptotic one, in the limit of a large number of events/year, and adopting a non-asymptotic one e.g. leading to the Metastatistical Extreme Value Distribution (MEVD, Marani and Ignaccolo, 2015). The MEVD has been widely applied to rainfall (Zorzetto et al., 2016) and, in particular, we use here the Simplified Metastatistical Extreme Value (SMEV) distribution (Marra et al., 2019) . The MEVD non-asymptotic approach assumes independent and identically Weibull-distributed ordinary events (Wilson and Toumi, 2005), within each year.

https://doi.org/10.5194/egusphere-2026-4418
Preprint. Discussion started: 30 July 2026
© Author(s) 2026. CC BY 4.0 License.

SMEV further assumes full stationarity. i.e. neglecting possible inter-annual variability, such that a single Weibull distribution of magnitudes may be fitted across all years.

Regionalization

Monthly hazard estimation is only as reliable as the sample behind it: this section establishes whether the four gauges may be treated as one sample. Splitting the record into month blocks leaves a limited number of ordinary events in each block, so that fitting the Weibull distribution separately at each gauge would carry a large sampling uncertainty. The standard remedy is regional frequency analysis (Hosking and Wallis, 1997): gauges sharing the same precipitation regime are treated as a single homogeneous region and their events are pooled, so that parameter estimation borrows information across space rather than relying on the short local record alone. Pooling is legitimate only if the gauges are statistically homogeneous, and homogeneity must be verified for the quantity that is actually pooled. In the present framework that quantity is the set of ordinary events of a given month block and duration, and not the annual maxima: the SMEV marginals are estimated from the ordinary events themselves (Section 2.2.1, Eq. 12). Homogeneity was therefore assessed directly on the ordinary events, separately for each month block and for each of the durations considered (10, 30, 60, 180 and 360 min). This choice also avoids a subtler difficulty: the annual sample of a gauge is a mixture of events belonging to different seasons, so two gauges may share the same annual distribution while differing month by month.

The comparison between gauges is based on L-moments, which are summary statistics analogous to the conventional mean, variance and skewness, but computed from linear combinations of the ordered observations and therefore far less sensitive to individual outliers (Hosking and Wallis, 1997). Of particular interest is the L-coefficient of variation, $t = L_2/L_1$, a dimensionless measure of the relative spread of the event depths. For the two-parameter Weibull distribution assumed for ordinary events (Section 2.2.1) the L-CV takes the simple form $t = 1 - 2^{-1/k}$, which depends on the shape parameter k alone and is independent of the scale parameter λ. Comparing the L-CV across gauges is thus equivalent to comparing their Weibull shape parameters, that is, the tail behaviour that SMEV extrapolates towards long return periods, irrespective of whether one gauge is simply wetter than another.

Regional homogeneity was then quantified through the Hosking–Wallis heterogeneity measure H, in the form adopted for ordinary events within the metastatistical framework by Devò et al. (2025). The measure compares the observed dispersion of the at-site L-CV values around their regional average with the dispersion that would be expected if all gauges shared a common parent distribution. The reference dispersion is obtained by simulating a large number of synthetic regions from a single regional Weibull distribution, each synthetic gauge being assigned the same number of events as the corresponding real one, so that record length is automatically accounted for. H is the difference between the observed and the mean simulated dispersion, standardised by the standard deviation of the latter. Following Hosking and Wallis (1997), a region is regarded as acceptably homogeneous when $H < 1$, possibly heterogeneous when $1 \leq H < 2$, and definitely heterogeneous when $H \geq 2$; negative values indicate gauges that are more similar to one another than repeated sampling from a common distribution would typically produce.

https://doi.org/10.5194/egusphere-2026-4418
Preprint. Discussion started: 30 July 2026
© Author(s) 2026. CC BY 4.0 License.

Because the SMEV marginals are not fitted to all ordinary events but only to those exceeding the q-th quantile of the empirical depth distribution — a left-censoring step that suppresses the influence of the weakest events on the Weibull tail fit, described in Section 2.2.1 and calibrated in Section 3.1.5 — the L-CV, and hence H, were computed on the censored sample, so that the test probes exactly the portion of the event population used by the frequency model. Under left censoring the relation between the L-CV and the shape parameter has no closed form and was evaluated numerically. As a complementary, distribution-free check, the censored ordinary-event tails of every pair of gauges were also compared through two-sample Kolmogorov–Smirnov (KS) tests, applied above a common depth threshold so that all gauges are compared over the same range. The KS statistic D is the largest vertical distance between the two empirical cumulative distribution functions of the pair, and the associated p-value is the probability of observing a distance at least as large if the two samples were drawn from the same distribution: small p-values therefore indicate gauges that cannot be pooled. Since several gauge pairs are compared within each month block and duration, and testing many pairs inflates the chance that at least one appears significant by accident, the p-values were also assessed against a Bonferroni-corrected significance level, obtained by dividing the nominal level by the number of pairs tested. The two tests are complementary: H constrains the shape of the distribution, whereas the KS test on the observed depths constrains both its shape and its magnitude.

Moreover, both regionalized (REG), and at-site (ATSITE) information was evaluated by analysing the extreme rainfall estimation performance. For both ATSITE and REG information, extreme rainfall quantiles were estimated using the SMEV model and evaluated through 3 complementary performance indicators. First, sampling robustness was evaluated by analysing the effective sample size, defined as the average number of independent maxima available for each station–season–duration combination. Second, the statistical reliability of the estimated extremes was quantified using a bootstrap approach, computing the relative width of the confidence interval of the 100-year return level for the 60 min duration. Finally, the ability of the stochastic model to reproduce inter-duration dependence was assessed through the mean absolute difference between simulated and observed Kendall's τ coefficients (see Section 2.2.1).

Ensemble of realistic synthetic storms: Multiduration dependence modelling with a C-vine copula

A crop is not damaged by a rainfall depth at one duration, but by the whole event: this section describes how depths at different durations are simulated jointly rather than independently. The role of the copula model that is here illustrated is not to generate a design storm shape directly, but to generate physically consistent rainfall-depth vectors across nested durations. These vectors define how rare rainfall accumulations at short and longer durations can co-occur within the same storm, which is essential because hydraulic response and crop damage depend on the whole event rather than on a single duration alone. The dependence between rainfall accumulations across different durations is modeled using a canonical Vine (C-Vine) copula, following the joint return-period framework introduced by Cache et al. (2025). However, the framework was modified to better suit a monthly-scale analysis. The approach exploits the fact that rainfall depths computed over nested temporal aggregations are not independent, but exhibit a structural dependence arising from storm dynamics.

Let $\mathbf{X} = \{X_{d_1}, \ldots, X_{d_n}\}$ denote the vector of rainfall depths associated with durations $d = \{d_1, ..., d_n\}$. According to Sklar's theorem, the joint distribution can be decomposed into marginal distributions and a copula describing their dependence struc-

https://doi.org/10.5194/egusphere-2026-4418
Preprint. Discussion started: 30 July 2026
© Author(s) 2026. CC BY 4.0 License.

ture. After transforming each marginal into uniform variables $U_d = F_d(X_d)$, the multivariate distribution can be written as

$$F(\mathbf{x}) = C(U_{d_1}, \ldots, U_{d_n}),$$

where C is approximated through a pair-copula construction.

The C-vine tree structure is defined based on the empirical dependence strength among durations, quantified through Kendall's rank correlation coefficient (τ). Durations are ordered according to their overall dependence with the remaining variables, such that the root node of the vine corresponds to the duration exhibiting the strongest aggregate rank correlation. This choice reflects the hierarchical nature of rainfall accumulations across nested time scales and ensures that dominant dependence relationships are captured in the first levels of the decomposition.

To avoid restrictive parametric assumptions on the copula families, the pair-copula components are estimated non-parametrically. In particular, the conditional distribution functions (so-called h-functions) are derived using a local linear kernel estimator based on the adjusted Nadaraya–Watson approach. This procedure provides a smooth estimate of the conditional cumulative distribution $P(U_i \leq u \mid U_j = v)$ directly from the data, improving stability near the boundaries of the unit interval and preserving the observed dependence structure without imposing a predefined copula family.

Synthetic duration–frequency vectors are generated through sequential conditional sampling along the vine structure. After sampling the root variable, subsequent durations are simulated conditionally using the estimated h-functions, thereby propagating dependence consistently across all time scales. In this study, the copula is estimated separately for homogeneous monthly groups in order to account for seasonal changes in storm structure.

Synthetic samples are conditioned on selected return periods. Differently from Cache et al. (2025), the conditioning is not restricted to a single reference duration: multiple anchor durations and return periods are considered, and bootstrap resampling of events exceeding the target return level is applied prior to copula fitting. This produces multiple equally plausible duration–frequency realizations reflecting both sampling uncertainty and natural variability in multiduration rainfall structure.

Event selection across the full spectrum of storm durations

A key methodological difference with respect to the framework of Cache et al. (2025) concerns the construction of the multivariate dataset used for the copula estimation. In that study, each precipitation event is represented by a fixed 360-min time window centred on the maximum 360-min accumulation, and only events whose actual wet duration spans the entire window contribute to the analysis. This ensures that all duration intervals are well resolved, but restricts the sample to long-duration events and may underrepresent storm types characterised by intense but shorter-lived rainfall, which are common during convective seasons.

Rainfall events are identified as independent wet periods separated by dry intervals of at least 24 hours, regardless of their duration. For each event, the maximum accumulation at every target duration $d \in \{d_1, \ldots, d_n\}$ is computed using a moving-window operator.

https://doi.org/10.5194/egusphere-2026-4418
Preprint. Discussion started: 30 July 2026
© Author(s) 2026. CC BY 4.0 License.

When the event duration is shorter than the target duration, the d-duration accumulation coincides with the total event rainfall, i.e.

$$X_d = \sum_{t=1}^{N_{\mathrm{ev}}} P_t, \qquad \text{if } N_{\mathrm{ev}} < d/\Delta t, \tag{11}$$

where N_{ev} is the number of time steps in the event, P_t is the rainfall depth at time step t, and Δt is the recording interval. This is equivalent to zero-padding the event outside its observed duration and implies that $X_{d_j} = X_{d_{j+1}}$ whenever the storm duration is shorter than d_{j+1}.

Including short events is important because some seasonal groups are dominated by short-lived convective storms. Restricting the analysis to events spanning the full 360-min window would substantially reduce the sample size and bias the dependence structure toward long-duration events. The resulting copula sample therefore includes both long events, characterized by increasing accumulations across durations, and short events, for which the accumulation saturates at the total event depth. This introduces rank ties along the upper boundary of the dependence structure, but the non-parametric h-function estimator remains robust because kernel smoothing naturally averages over neighbouring observations.

Unified copula–marginal framework with the SMEV distribution

A methodological difference with respect to Cache et al. (2025) lies in the choice of the marginal model. In that study, the marginals used to invert the copula pseudo-uniforms, $\tilde{x}_d = F_d^{-1}(\tilde{u}_d)$, are classical event-level parametric distributions (Lognormal or Gamma). Here, we instead adopt the Simplified Metastatistical Extreme Value (SMEV) distribution (Marra et al., 2019), which provides more reliable estimates of extreme quantiles by exploiting the full population of ordinary events rather than a single value per year. As in Cache et al. (2025), both the copula structure and the marginals are estimated from the same event dataset — here the ordinary events — so that the inversion is consistent with Sklar's theorem by construction.

The SMEV framework models the annual-maximum cumulative distribution function as the n-th power of the event-level Weibull CDF:

$$F_{\mathrm{AM}}(x) = \left[1 - \exp\left(-\left(\frac{x}{\lambda_d}\right)^{k_d}\right)\right]^n, \tag{12}$$

where λ_d and k_d are the Weibull scale and shape parameters for duration d, estimated from ordinary events via weighted linear regression with left-censoring below the q= 0.6 quantile (See Section 3.1.5), and n is the mean annual number of independent events. Crucially, because each precipitation event is isolated once and the maximum accumulations at all target durations are extracted from the same event window, the parameter n is identical across all durations. Only the Weibull parameters λ_d and k_d vary with duration, reflecting the increasing rainfall accumulations at longer time scales.

The C-vine structure and h-functions are estimated from the normalised ranks of these same ordinary events, yielding pseudo-uniform variables $\tilde{u}_d \in (0,1)$ for each duration d. Since the copula and the marginals share the same underlying sample, the mapping between $\tilde{u}_d$ and physical rainfall depths is exact—no intermediate probability-space transformation is required.

https://doi.org/10.5194/egusphere-2026-4418
Preprint. Discussion started: 30 July 2026
© Author(s) 2026. CC BY 4.0 License.

The inversion from copula uniforms to physical rainfall depths admits a closed-form expression due to the shared-n structure of the SMEV model. The annual-maximum quantile function corresponding to Equation (12) is

$$\tilde{x}_d = \lambda_d \left[-\ln\left(1 - \tilde{u}_d^{1/n}\right)\right]^{1/k_d}. \tag{13}$$

Here, $\tilde{u}_d^{1/n}$ maps the annual-maximum non-exceedance probability to the corresponding event-scale probability. Since the parameter n is shared across all durations, the same probability level is applied consistently to every duration, while the scaling is controlled by the duration-dependent SMEV parameters (λ_d, k_d). For rainfall data, these parameters typically increase monotonically with duration, ensuring that

$$\tilde{x}_{d_j} \leq \tilde{x}_{d_{j+1}}, \qquad d_j < d_{j+1},$$

without requiring post-processing corrections.

The analytical form of Equation (13) avoids the need for numerical root-finding and yields computational costs comparable to standard parametric marginals.

Conversely, the forward transformation from rainfall depth to copula space is

$$u_d = F_{\mathrm{AM}}(x_d) = \left[1 - \exp\left(-\left(\frac{x_d}{\lambda_d}\right)^{k_d}\right)\right]^n. \tag{14}$$

This formulation preserves the separation between the dependence structure, modelled by the copula on the rank scale, and the marginal behaviour, governed by the SMEV parameters (λ_d, k_d, n).

Temporal disaggregation: micro-canonical cascade model

The copula provides the rainfall amounts associated with multiple durations, but it does not specify the internal temporal organization of the event. A microcanonical cascade is used to generate sub-event temporal structures that conserve the total simulated event depths, while allowing for a variety of temporal rainfall structures and intermittent bursts. The copula–SMEV framework described above provides, for each simulated event, a vector of rainfall depth values $\tilde{\mathbf{x}} = \{\tilde{x}_{d_1}, \ldots, \tilde{x}_{d_n}\}$ consistent with the observed duration–frequency dependence structure. These depths must then be disaggregated into a continuous precipitation time series at the base time step Δt. To this end, we adopt a bounded micro-canonical multiplicative random cascade model, following Olsson (1998) and Cache et al. (2025), which guarantees exact conservation of the precipitation depth throughout the disaggregation process, such that accumulations at each target duration match the copula-sampled depths (Cache et al., 2025).

Starting from a single box of duration equal to the entire rainfall event, the multiplicative random cascade process successively subdivides the initial total rainfall depth into finer time steps through a sequence of disaggregation levels $\ell = 1, \ldots, L$. At each level, a parent box is split into b_ℓ child boxes, where b_ℓ is either 2 or 3 depending on the level, following the scheme of Cache et al. (2025): for example, starting from a 360 min rainfall event, the parent depth is halved ($b_\ell = 2$) in the 360–180 min and 60–30 min transitions, while a threefold split ($b_\ell = 3$) is required in the 180–60 min and 30–10 min transitions, so that the cascade passes through all the target durations of the analysis (10, 30, 60, 180, and 360 min).

https://doi.org/10.5194/egusphere-2026-4418
Preprint. Discussion started: 30 July 2026
© Author(s) 2026. CC BY 4.0 License.

For the $b_\ell = 2$ levels, a stochastic multiplier, W, determines the fraction of the parent depth assigned to the left child box, so that the right child box receives $1 - W$. A pair of weights can assume one of three states:

$$(W_1, W_2) = \begin{cases} (1,\ 0) & P(1{,}0) \\ (0,\ 1) & P(0{,}1) \\ (W,\ 1-W),\ W \sim F_W & P(W{,}1-W) \end{cases} \tag{15}$$

where F_W is the empirical cumulative distribution of the continuous weight $W \in (0,1)$, estimated from the observed events aggregated to the temporal resolution of level ℓ. The parameters $\{P(1,0),\, P(0,1),\, P(W,1-W),\, F_W\}$ are estimated separately at each disaggregation level (bounded cascade, Müller-Thomy, 2020; Müller and Haberlandt, 2018). For the $b_\ell = 3$ levels, the parent depth is split among three child boxes, and the weight triplet can assume one of seven states:

$$(W_1, W_2, W_3) = \begin{cases} \text{state} & \text{probability} \\ (1,0,0) & P(1{,}0{,}0) \\ (0,1,0) & P(0{,}1{,}0) \\ (0,0,1) & P(0{,}0{,}1) \\ (W, 1-W, 0) & P(W{,}1-W{,}0) \\ (W, 0, 1-W) & P(W{,}0{,}1-W) \\ (0, W, 1-W) & P(0{,}W{,}1-W) \\ (W, V, 1-W-V) & P(W{,}V{,}1-W-V) \end{cases} \tag{16}$$

where $W \sim F_W$ is the fraction assigned to the first wet child box and, when all three child boxes are wet, $V \sim F_{V|W}$ is the fraction assigned to the second child box, with $W + V \leq 1$. As in the $b_\ell = 2$ case, the state probabilities and the empirical distributions F_W and $F_{V|W}$ are estimated separately at each disaggregation level (Lisniak et al., 2013; Cache et al., 2025).

Left-sibling wet/dry conditioning.

Observed gap-duration distributions and the number of dry spells per event suggest that the occurrence of a dry period in the cascade is not independent of the state of the immediately preceding time interval. In particular, periods of zero rainfall tend to cluster, implying that the probability of a sibling box being dry is higher when the preceding sibling is also dry (Müller-Thomy, 2020). Standard cascade models, which sample the weight states in Equation (15) independently at each split, cannot represent this persistence, leading to an excess of short isolated gaps and an underestimation of the frequency of events with few long dry spells. To introduce wet/dry memory, we implemented and tested a left-sibling conditioning following Müller and Haberlandt (2018). At each $b_\ell = 2$ branching, let $\mathcal{S}_{j-1}^{(\ell,e)} \in \{\mathrm{wet}, \mathrm{dry}\}$ denote the state of the sibling block immediately to the left of block

https://doi.org/10.5194/egusphere-2026-4418
Preprint. Discussion started: 30 July 2026
© Author(s) 2026. CC BY 4.0 License.

j for event e. The discrete probabilities in Equation (15) are then conditioned on this state:

$$P\left(W_1, W_2 \,\middle|\, \mathcal{S}_{j-1}^{(\ell,e)}\right) = \begin{cases} P^{\mathrm{lw}}(W_1, W_2) & \text{if } \mathcal{S}_{j-1}^{(\ell,e)} = \mathrm{wet}, \\ P^{\mathrm{ld}}(W_1, W_2) & \text{if } \mathcal{S}_{j-1}^{(\ell,e)} = \mathrm{dry}, \end{cases} \tag{17}$$

where P^{lw} and P^{ld} are estimated separately from all observed parent boxes at level ℓ whose left sibling was wet or dry, respectively. Note that the conditioning acts only on the discrete state probabilities $\{P(1,0), P(0,1), P(W, 1-W)\}$; in all states the weights satisfy $W_2 = 1 - W_1$, so that mass conservation is preserved, and the distribution F_W of the continuous weight is left unconditioned. Persistence is not imposed a priori: the conditional probabilities are estimated empirically, and wet/dry clustering in the observations translates into $P^{\mathrm{ld}}(0,1) > P^{\mathrm{lw}}(0,1)$, that is, an increased probability that the child box adjacent to a dry neighbour is itself dry. For blocks without a left sibling (i.e., the leftmost box at each level), the unconditional parameters from Equation (15) are used.

2.2.2 Hydrological–hydraulic model

The hydrological-hydraulic model provides the physically-based link between rainfall events and crop damage. The model converts generated hyetographs into spatial water depth distributions and calculates inundation durations, which are the hazard variables required as input to the crop damage functions. Flood dynamics were simulated using a fully two–dimensional model based on *HEC-RAS v. 6.6.*. The model solves the depth-averaged shallow water equations in conservative form over a computational mesh using a finite-volume scheme, and provides a process-based representation of flow routing, storage, and lateral spreading over complex topography.

Rainfall–runoff generation is represented through an event-based approach in which effective precipitation is derived from total rainfall using the SCS–Curve Number (SCS–CN) infiltration method. Synthetic hyetographs derived from the pooled regional statistics were applied as spatially uniform rainfall over the catchment, an assumption justified by its small extent and by the homogeneity of the gauges (Section 3.1.1). The resulting surface runoff is directly applied to the 2D computational domain as a spatially-distributed source term, thus coupling hydrological and hydraulic processes within a single modelling framework. The hydraulic component simulates unsteady flow propagation, surface ponding, and floodplain storage driven by local topographic gradients and hydraulic connectivity. Momentum exchange between cells accounts for backwater effects, flow redistribution, and temporary depressions typical of low-relief environments. This configuration enables the direct simulation of pluvial flooding processes, where inundation is primarily controlled by rainfall excess and limited drainage capacity rather than river-floodplain flow exchange.

2.3 Exposure and vulnerability

The results of the hydrological-hydraulic model must be translated into agricultural impacts by considering crop exposure and vulnerability. Exposure is a function of which crops are present in each month, while vulnerability determines how damaging a given combination of flood depth and duration is for the phenological stage reached by each crop. Both exposure and vulnerability components are here recognized to be dependent on the month in which the event occurs, to fully account for their

https://doi.org/10.5194/egusphere-2026-4418
Preprint. Discussion started: 30 July 2026
© Author(s) 2026. CC BY 4.0 License.

seasonality. For each crop c and month m, exposure is defined as the cultivated area $A_{m,c}$ potentially affected by flooding. This area is assumed to be constant during the corresponding crop-calendar period and equal to zero in months in which the crop is not present in the field. Crop vulnerability is represented through crop-specific depth–duration damage functions that depend on flood water depth, inundation duration, and phenological stage. For each return period T_i, the hydraulic simulations provide spatially-distributed flood depths and durations, which are combined with the relevant damage curve for crop c and month m to estimate the dimensionless damage fraction $d_{c,m}(T_i)$. This formulation allows the same flood event to produce different damage levels depending on the timing of occurrence within the growing season, thereby linking flood hazard dynamics with crop exposure and phenological sensitivity.

3 Case study and Data

The study area is the Ceresolo drainage basin upstream of the city of Rovigo (Veneto region, north–eastern Italy), with an area of approximately 56 km^2 (Fig. 2). The basin is part of the low-lying Po River plain reclamation system and is almost entirely cultivated. The Ceresolo channel is an artificial drainage and irrigation collector.

The catchment is characterised by gentle bed slopes (about 22 $\mathrm{cm\,km^{-1}}$ upstream of Rovigo), typical of reclaimed alluvial plains, resulting in limited hydraulic conveyance capacity and high sensitivity to short-duration intense rainfall. The drainage network consists of a system of artificial canals managed by the reclamation consortium (*Consorzio di Bonifica Adige-Po*), collecting runoff from multiple sub-basins and routing it towards downstream pumping stations.

Due to the flat topography and long flow paths, runoff concentration times are relatively large and water levels are strongly controlled by the drainage infrastructure. Under intense precipitation, the system frequently experiences drainage inefficiency and temporary waterlogging of cultivated fields. For this reason, the area is a representative case of agricultural flood risk in artificial lowland basins where damage is primarily caused by surface ponding rather than river overflow.

https://doi.org/10.5194/egusphere-2026-4418
Preprint. Discussion started: 30 July 2026
© Author(s) 2026. CC BY 4.0 License.

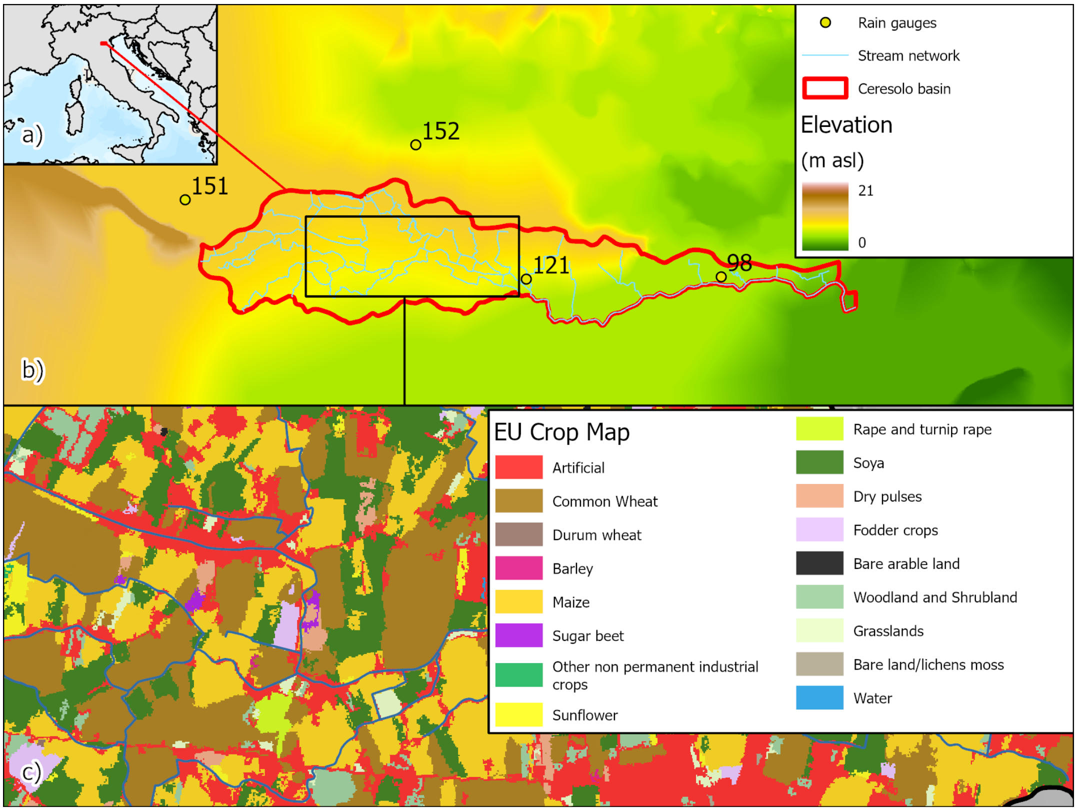

Figure 2. a) Location of the study area in Italy. b) Boundaries of the Ceresolo river basin with the location of the rain gauges. c) a detail of the distribution of crops in the study area

420 ### 3.1 Application of the statistical method for the generation of the synthetic hyetographs

Rainfall observations were obtained from the regional monitoring network operated by the Veneto Environmental Protection Agency (*ARPAV*), providing continuous quality-controlled measurements recorded at 5 min temporal resolution with 0.2 mm depth resolution from heated tipping-bucket rain gauges.

3.1.1 Regionalization on the case study

The regional homogeneity evaluation described in Section 2.2.1 was performed using four gauges located in the proximity of the catchment (Fig. 2). The four rain gauges lie a few tens of kilometres apart and at similar elevations, sharing the same precipitation-generating regime. Depending on the month, each gauge contributes between 92 and 171 ordinary events, thereby leading to 37 to 84 events above the 60th percentile threshold adopted in the left-censoring method to fit the marginal distribution. The regional Weibull shape parameter varies between 0.71 and 1.25 across months and durations (Table S2). Shape values below unity correspond to sub-exponential, heavier-than-exponential tails, in which the probability of very large event depths decays more slowly than an exponential distribution; such tails are typical of short-duration convective storms. Conversely,

https://doi.org/10.5194/egusphere-2026-4418
Preprint. Discussion started: 30 July 2026
© Author(s) 2026. CC BY 4.0 License.

values above unity indicate lighter-than-exponential tails, characteristic of longer-duration stratiform precipitation associated with large-scale dynamics (Wilson and Toumi, 2005; Andria et al., 2025). The estimated parameters thus follow the expected seasonal gradient, from heavy-tailed convective events in summer to lighter-tailed stratiform precipitation in winter.

Across the 60 combinations of month and duration, the heterogeneity measure computed on the censored ordinary events remains below unity in 56 cases, and no combination reaches the threshold $H \geq 2$ that would indicate a conclusively heterogeneous region (see in the Supplement Fig. S1, Tables S1 and S2). The four remaining cases fall in the intermediate, "possibly heterogeneous" range and occur in December and February. The pairwise KS tests confirm this picture: the six gauge pairs were tested separately for each of the 60 month and duration combinations, for a total of 360 tests. Only in two of the 360 tests is the null hypothesis of a common distribution rejected at the nominal $\alpha = 0.05$ level. This is fewer than the $\sim$18 rejections expected by chance alone when 360 independent tests are performed at the 5% level. Accordingly, after a Bonferroni correction for multiple comparisons — which controls the family-wise error rate by lowering the per-test significance threshold to $\alpha/360 \approx 1.4 \times 10^{-4}$ — no rejection remains, and the largest KS statistic across all tests is $D = 0.282$. For the sample sizes involved ($n \approx 37$–84 censored events per gauge and month), this value is comparable to the $\alpha = 0.05$ critical value of the two-sample KS test, $D_{\mathrm{crit}} = c(\alpha)\sqrt{(n_1+n_2)/(n_1 n_2)} \approx 0.21$–0.32 (Massey, 1951), and well below the Bonferroni-adjusted critical values (≈ 0.34–0.51): even the largest observed discrepancy between empirical distributions is within the range expected from sampling variability alone.

On this basis, the regional (REG) configuration was preferred over the at-site (ATSITE) one, considering the better values of confidence interval width, sample size, and difference between simulated and observed Kendall's coefficients for every month (Fig. S2).

3.1.2 Testing of the SMEV distribution as the marginal model against conventional parametric distributions

The suitability of the SMEV distribution as a marginal model was systematically evaluated against a set of conventional parametric distributions, namely Burr XII, Log-logistic, Pearson type III, Gamma, and Lognormal. Although the SMEV distribution is specifically derived for extreme value modeling, it is here also assessed for its ability to reproduce the full probabilistic structure of rainfall, including ordinary (i.e., non-extreme or moderate extreme) events. Note that this analysis was done by choosing the ordinary-event filtering and left censoring thresholds discussed in the following sections.

The five candidate distributions for event-level precipitation depths were selected to span a broad range of tail behaviors documented in the extreme precipitation literature. The Gamma and Lognormal distributions are widely adopted parametric models in stochastic storm simulation frameworks (Cache et al., 2025) and are among the most commonly used distributions in precipitation frequency analysis globally (Papalexiou and Koutsoyiannis, 2016). The Burr Type XII (BurrXII) distribution was explicitly recommended by Papalexiou and Koutsoyiannis (2016) on the basis of a global survey of over 1.7×10^5 monthly daily precipitation records, outperforming exponential-tail models in reproducing the heavy-tailed behaviour of precipitation extremes. The Pearson Type III (PearsonIII) distribution is a flexible three-parameter model widely applied to rainfall and flood frequency analysis in both national standards and international studies (Griffis and Stedinger, 2007; Hosking and Wallis, 1997).

https://doi.org/10.5194/egusphere-2026-4418
Preprint. Discussion started: 30 July 2026
© Author(s) 2026. CC BY 4.0 License.

The Log-Logistic distribution has been applied to extreme rainfall frequency analysis at the regional scale (Sharda et al., 2008; Fitzgerald, 2005) and provides power-law tail decay, bridging the behaviour of Lognormal and Pareto-type models.

The comparison was carried out following two complementary approaches. First, an in-sample evaluation was performed to assess how well each distribution reproduces the empirical probability structure of the observations across a range of return periods (2, 10, 50, and 100 years) for all considered durations (Fig. S3). Results indicate that, for low return periods (e.g., 2 years), the SMEV distribution provides an effective fit, on average, with performance slightly lower to the best-performing distribution (Burr XII). For higher return periods (10, 50, and 100 years), the SMEV outperforms the alternative distributions, exhibiting lower relative mean errors across most durations.

Second, a cross-validation framework was implemented, following the approach proposed by Zorzetto et al. (2016), to evaluate the generalization ability of each distribution. In this out-of-sample setting, the SMEV consistently shows superior performance compared to the other candidate distributions in the majority of cases, with the exception of the 10 min duration quantiles for which Pearson III and Gamma show better performances (Fig. S5).

Overall, these results highlight the robustness of the SMEV distribution not only in modeling extreme rainfall but also in adequately representing lower-probability, ordinary events, supporting its use as a unified marginal model across the full range of storm magnitudes.

3.1.3 Event selection across the full spectrum of storm durations

The empirical cumulative distribution function of observed event durations (Fig. S6) shows that extreme events shorter than the 6-hour window are not negligible: in the summer months, dominated by convective storms, they account for almost 40% of the extreme events. Their inclusion must therefore be weighed against a possible cost in fitting performance, which turns out to be negligible. The mean absolute error (MAE) of Kendall's τ between observed and vine-copula-simulated events is comparable in the two configurations and, in 7 out of 12 months, it is actually lower when short events are included (Fig. S7b), indicating that the additional events do not distort the inter-duration dependence structure. Likewise, the root mean square error (RMSE) of the 50-year return level is comparable in the two configurations, both in out-of-sample cross validation (Fig. S7c) and in-sample (Fig. S7d): including short events yields slightly larger errors at the shortest durations and slightly smaller errors at the longest ones. Note, however, that each configuration is evaluated against its own observed sample: when short events are excluded, the sample used for validation itself omits all observed extremes shorter than 6 hours. The slightly lower short-duration RMSE of the exclusion configuration is thus achieved on a reduced event population, at the cost of neglecting up to 40% of the extreme events that actually occurred. Since including short events entails no appreciable loss in either the dependence or the marginal performance, while ensuring that all observed extremes contribute to the analysis, they were retained.

3.1.4 Choice of the ordinary-event filtering threshold for the SMEV-copula framework

The unified SMEV–copula framework described in Section 2.2.1 requires a consistent ordinary-event dataset for both marginal fitting and copula estimation. Because the full set of ordinary events includes a large proportion of weak, low-intensity episodes,

https://doi.org/10.5194/egusphere-2026-4418
Preprint. Discussion started: 30 July 2026
© Author(s) 2026. CC BY 4.0 License.

the dependence structure inferred from the complete sample may poorly represent the behaviour of significant rainfall events, leading to systematic mis-representation of inter-duration Kendall's τ coefficients in the upper tail. At the same time, restricting the dataset to events above an excessively high return-period threshold progressively reduces the sample size available for marginal fitting, degrading the statistical reliability of the estimated extreme quantiles. To characterize this trade-off, ordinary events were filtered according to a minimum event-level return period threshold $\rho_{\min}$, defined consistently with the SMEV framework as

$$\mathrm{RP}_{\mathrm{event}}(x) = \frac{1}{\bar{n}\left[1 - F_{\mathrm{event}}(x)\right]}, \tag{18}$$

where $F_{\mathrm{event}}(x) = 1 - \exp\left[-(x/\lambda)^k\right]$ is the Weibull event-level cumulative distribution function and $\bar{n}$ is the mean annual number of ordinary events. This formulation expresses the expected recurrence interval of a single event of depth x in years, and is sub-annual for the bulk of the ordinary event population. An event is retained if its event-level return period exceeds $\rho_{\min}$ in at least one of the target durations.

The sensitivity of the results to the choice of $\rho_{\min}$ was evaluated by considering two aspects: the reproduction of the Kendall's τ matrix of the unconditioned copula model against observations, and the reproduction of empirical quantiles in both in-sample and out-of-sample tests. Fig. S8 shows the mean absolute error (MAE) of the pairwise differences $\Delta\tau$ between the Kendall's τ of observed events and that of unconditional samples from the fitted C-vine copula, as a function of the filtering threshold $\rho_{\min}$, expressed as an event-level return period. The MAE is largest at the two ends of the tested range, that is, for thresholds close to 0 years (nearly all ordinary events retained) and close to 1 year (only the rarest events retained). This behaviour reflects two opposite effects: with a low threshold, the abundant weak events distort the dependence structure among the maximum accumulations at different durations, whereas with a high threshold the SMEV marginals are fitted to too few events, degrading their reliability. The MAE reaches its minimum for $\rho_{\min}$ between 0.4 and 0.5 years. With this choice, the copula performance is comparable to — and for most months better than — that obtained with the approach of Cache et al. (2025), in which no ordinary-event filtering is applied and a Gamma distribution, instead of the SMEV, is used as the marginal model (Fig. S8). Among the two candidate marginals tested by Cache et al. (2025), the Gamma distribution was adopted here as it provided a better fit than the Lognormal for the events of the study area, consistently with their treatment of the marginal distribution as a user-defined choice.

Regarding the sensitivity of the ordinary events threshold performance in calculating the quantiles, the in-sample root mean square error (RMSE) of the SMEV-estimated quantiles against the empirical annual maxima was computed for return periods spanning the range $T = 2$–100 years (Fig. S9). Second, the cross-validated RMSE following the methodology of Zorzetto et al. (2016) was used to assess out-of-sample performance in the extrapolation regime (Fig. S10). Results indicate that low values of $\rho_{\min}$ (baseline: all ordinary events) yield the smallest RMSE at short return periods but the largest errors for rare events, as the fitted Weibull tail is pulled towards the bulk of the distribution. Conversely, high filtering thresholds improve the reproduction of extreme quantiles at the cost of degraded performance at ordinary return periods and, for short durations, also in cross-validation.

https://doi.org/10.5194/egusphere-2026-4418
Preprint. Discussion started: 30 July 2026
© Author(s) 2026. CC BY 4.0 License.

A threshold of $\rho_{\min} = 0.4$ years was identified as a compromise across durations and seasons, balancing adequate marginal quantile estimation with improved inter-duration dependence reproduction as measured by the MAE of Kendall's τ. The mean annual event frequency $\bar{n}$ is recomputed from the filtered sample after applying the threshold, ensuring that the SMEV annual-maximum CDF remains consistent with the effective event rate in the dataset used for fitting. Correspondingly, the C-vine copula is estimated from the same filtered dataset, so that the Sklar decomposition remains exact by construction.

3.1.5 Choice of the left-censoring proportion

The SMEV marginal fitting employs left-censoring of ordinary events below the q-th quantile of the empirical depth distribution, following Marra et al. (2019). This censoring suppresses the influence of the weakest events on the Weibull tail fit, improving the estimation of extreme quantiles. However, the optimal censoring proportion q is not universal: an excessively high q risks discarding events that carry information about the distributional shape, while a too-low q re-introduces the bias from weak events that censoring is designed to remove.

The sensitivity of the framework to the left-censoring proportion was evaluated by computing the SMEV quantile RMSE as a function of $q \in [0, 1)$ for each month and duration separately. This analysis reveals that the optimal q varies significantly across months, durations, and return periods (Fig. S11). Specifically, for a low return period (i.e. 2 years) very low values (0-0.1) of the left censoring threshold minimize the RMSE with respect to observed quantiles for summer months across all durations, while higher values of the left censoring thresholds (0.6-0.95) perform better in the other seasons. For a high return period (100 years), with the exception of a few cases, high values of the left censoring percentile lead to a better performance. A value of $q = 0.6$ was chosen as a compromise to accurately estimate lower and higher magnitude rainfall quantiles. This value was therefore adopted uniformly across all months, with the understanding that month-specific tuning could further reduce errors in individual seasons.

3.1.6 Copula-based storms definition

The three configuration choices described above—inclusion of short-duration events, the ordinary-event filtering threshold $\rho_{\min}$, and the left-censoring proportion q—are not independent: each influences the effective sample size and the empirical distribution of depths available for fitting. The choice was therefore conducted iteratively, reassessing the sensitivity of each parameter conditional on the values selected for the others, until convergence to a configuration that performed consistently across all diagnostics. As an example of how extremes change as a function of the month being considered, Fig. S12 shows the radar plot of the rainfall quantiles and their relative uncertainties calculated with the bootstrap procedure proposed by Marra et al. (2019) varying different durations for a return period equal to 100 years. Note that quantiles from July for durations equal to or higher than 3 hours are even higher with respect to those determined using the entire annual dataset (dashed black line), but with much higher uncertainty. On the other hand, winter months provide much lower extreme values with respect to the annual computation. This means that the severity of an extreme event, such as the 100-year return period, can dramatically change among months, even by a factor of 10, depending on the crop exposure and vulnerability. On the other hand, the relatively smaller sample size of a monthly analysis of extreme rainfall, with respect to the traditional annual analysis, leads

https://doi.org/10.5194/egusphere-2026-4418
Preprint. Discussion started: 30 July 2026
© Author(s) 2026. CC BY 4.0 License.

to much higher uncertainties. This effect is also evident in the probability-distribution fits to the tails of the observed extreme events (Fig. S4). Because the July sample contains fewer events, the most extreme convective storms exert a stronger influence on the fitted upper tail. Their influence is less pronounced in the annual dataset, which includes a much larger number of lower-magnitude events that constrain the overall fit. The pairwise Kendall's τ values simulated by the unconditioned SMEV-based C-vine copula are generally in close agreement with the observed values across duration ratios (Fig. S13). However, the discrepancies become more pronounced during autumn and winter, particularly at larger duration ratios, when events are longer and less numerous. The smaller sample size therefore reduces the robustness of the estimated dependence structure and, consequently, the model's ability to reproduce the observed Kendall's τ. For comparison, the dependence analysis was repeated using the original approach of Cache et al. (2025), in which Gamma distributions are adopted for the marginals. This configuration produces slightly lower simulated dependence values across seasons. The difference arises because retaining unfiltered ordinary events leads to a more regular dependence structure across durations than that obtained from the subset of events with multi-year return periods. Based on 1000 simulations, storm variability across different durations and months is shown in Fig. 3 for a 100 years return period. In each column, the 100-year rainfall quantile is defined for a specific reference duration. The corresponding storm characteristics at the other durations are then shown for three individual months in each row, with one coloured boxplot for each month. At the reference duration, the spread of the simulated rainfall depths reflects the sampling uncertainty of the 100-year quantile, as estimated through bootstrap resampling. The relation of rainfall values among different durations for the same rainfall extreme event is strongly variable across months. For example, during winter, when the 100-year return level is defined at the 10-min duration, the corresponding rainfall depths at 3- and 6-h durations span a wide range. This indicates that a very extreme short-duration event may be associated with markedly different rainfall accumulations over longer time windows. In summer, by contrast, rainfall depths vary much less across durations. This suggests that many summer extremes are concentrated within short time intervals, with little additional rainfall accumulating during the remainder of the 3- or 6-h window. This behaviour is consistent with short-lived convective storms, for which most of the total rainfall accumulation occurs within a limited portion of the longer observation window. Ranges of return periods of rainfall quantiles for several return periods on selected durations are reported in Tab. S3.

3.1.7 Cascade model application

The cascade model was applied to generate 100 profiles for each of the 1000 elements of the copula-derived sample. The distributions of the rainfall peak depth location at the finer disaggregation level of the observed and simulated rainfall events for a reference storm duration of d*=360 min and a design return period of T=100 yr are reported in Fig. 4. The constrained micro-canonical cascade model slightly underestimates the occurrence of front-loaded events in summer and spring months, but generally they reproduce well the different seasonal shape of the hyetograph structure that may impact on the propagation of runoff depth on the basins surface. Moreover, the left-sibling conditioning illustrated in the methodology section was implemented and evaluated against the diagnostics reported in Fig. S14. The improvements in the gap-duration and gap-count distributions were not relevant. This outcome is probably due to the fact that reproducing the autocorrelation structure of rainfall - which is closely related to intermittency persistence - requires an extended position-dependency formulation rather

https://doi.org/10.5194/egusphere-2026-4418
Preprint. Discussion started: 30 July 2026
© Author(s) 2026. CC BY 4.0 License.

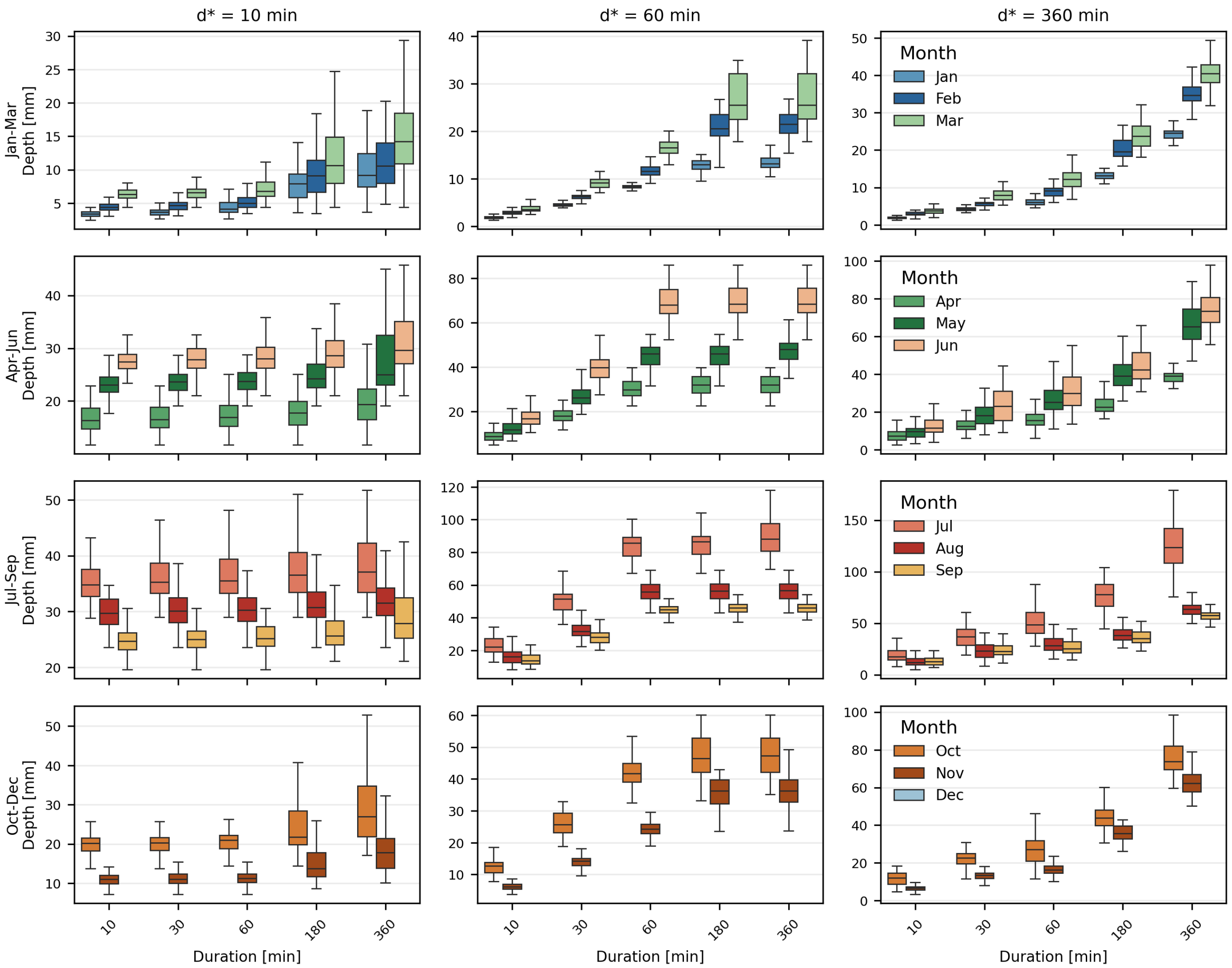

Figure 3. Distribution of simulated rainfall depths generated by the copula-based storm generator for a return period of 100 years. Boxplots show conditional rainfall depths across durations for three reference durations (d = 10, 60, and 360 min; columns). Rows correspond to quarterly groups of months (Jan–Mar, Apr–Jun, Jul–Sep, Oct–Dec), while colors indicate individual months within each quarter. Each box summarizes the distribution of synthetic events generated by the model.

https://doi.org/10.5194/egusphere-2026-4418
Preprint. Discussion started: 30 July 2026
© Author(s) 2026. CC BY 4.0 License.

than a binary left-sibling state. These findings reflect structural constraints of the standard micro-canonical framework that cannot be resolved through local modifications to the parameter conditioning, and the experimental extension is therefore not retained in the final model configuration. Another limitation of the microcanonical model is the representation of the wet fraction at different durations (see Fig. S15). For all the months, especially during winter and autumn, the simulated hyetographs tend to increasingly overestimate the wet fraction with respect to the one derived from the observations as time resolution increases. Two complementary mechanisms contribute to this bias. First, parent boxes assigned to the continuous splitting state $(W, 1-W)$ produce two wet child boxes whenever both fractional depths exceed the wet/dry threshold (here 0.2 mm per base time step), even when the physical process is better represented by a fully concentrated $(1,0)$ or $(0,1)$ state. Second, the simulated profiles represented in Fig. S15 are conditioned on a design return period of $T = 5$ yr, implying large total event depths that increase the probability of both child boxes exceeding the threshold in any given split. As a result, the wet fraction curves derived from simulated profiles lie above the observed calibration curve at all levels, and the gap widens progressively toward the finest scale.

The dashed curves in Fig. S15 show the wet fraction computed on the subset of observed and simulated events obtained by excluding short-duration events from the calibration dataset (i.e., events shorter than 360 min). The small difference between the two configurations indicates that the overestimation of wet fraction is not driven by the inclusion of short events, but is instead an intrinsic property of the cascade splitting mechanism at fine temporal resolutions.

https://doi.org/10.5194/egusphere-2026-4418
Preprint. Discussion started: 30 July 2026
© Author(s) 2026. CC BY 4.0 License.

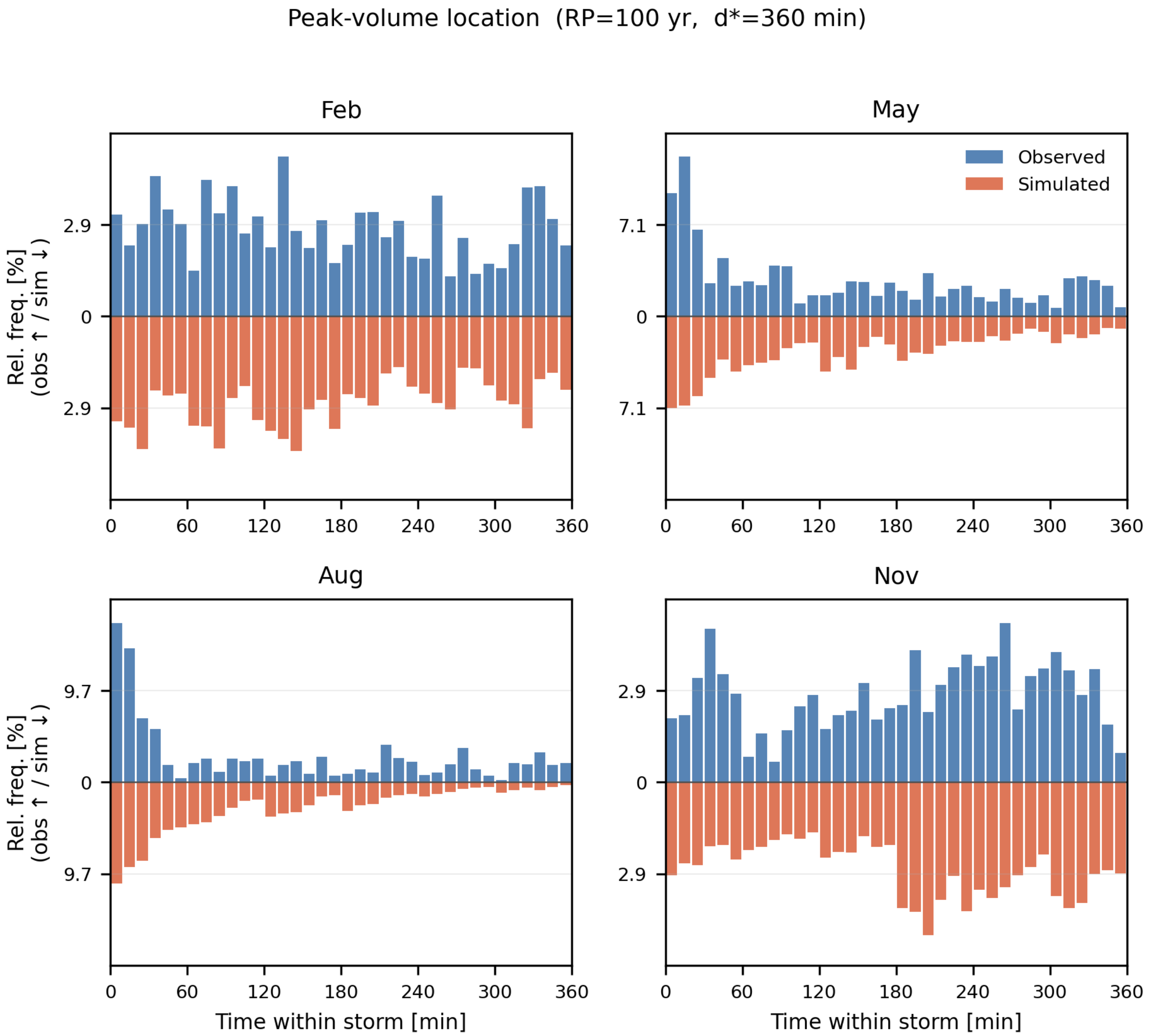

Figure 4. Distribution of the within-storm peak position for observed (blue) and simulated (orange) hyetograph profiles at the finest temporal resolution (base time step), shown for four representative months (February, May, August, November). The peak position is expressed in minutes from storm onset, for a reference storm duration of d*=360 min and a design return period of T=100 yr. Each panel reports the relative frequency histogram over all observed calibration events and over the ensemble of simulated profiles.

https://doi.org/10.5194/egusphere-2026-4418
Preprint. Discussion started: 30 July 2026
© Author(s) 2026. CC BY 4.0 License.

3.2 Implementation and validation of the hydrological-hydraulic model

Initial values of the curve-number parameters for the infiltration model were derived by intersecting the Corine Land Cover maps by the *Consorzio di Bonifica Adige-Po* and the hydrologic soil group maps derived from *ARPAV*. Antecedent Soil Moisture Conditions were fixed at condition II, medium wetness, on the basis of the frequency distributions of the antecedent 5-day rainfall, which was found to be below the AMC II threshold most of the time in all months. Floodplain topographic information for the hydraulic model was derived from the Digital Terrain Model of the Veneto region at 5 m spatial resolution. Channel cross sections of the Ceresolo canal and its tributaries were provided by the *Consorzio di Bonifica Adige-Po*. The distribution of the Manning values for the application of the hydro-dynamic model were derived from the HEC-RAS 2D User's Manual associating roughness conditions to Corine Land Cover values.

Model validation was performed by comparing observed flood extents, available from satellite data from recent floods, with modelled inundation maps. Water level time series at the Ceresolo channel provided by the *Consorzio di Bonifica Adige-Po* were visually inspected but not considered sufficiently reliable during flood events. The most intense rainfall events over the last 10 years were first identified and ranked according to their return period (based on extreme value analysis of observed rainfall). For these events, the availability of satellite data (Copernicus Sentinel-1 and 2, and Landsat) close to the flood peak was verified, leading to the selection of two recent events (July 2017 and July 2018, Fig. S16). For each selected event, the hydraulic model was forced using observed rainfall data and simulations were run in HEC-RAS to reproduce the flood dynamics. Rainfall observations were spatially interpolated with the inverse distance weighting technique. Modelled flood extent was extracted at the times of the satellite overpasses. Observed flood extent was derived from Sentinel-1 SAR imagery using a multi-temporal change-detection approach (Clement et al., 2018). For each event, the ratio between the pre-event and post-event backscatter was calculated, and pixels with a ratio greater than 1.2 were classified as potentially inundated. This criterion identifies areas characterised by a marked reduction in backscatter during the event, as expected for open-water surfaces. Finally, modelled and observed inundation extents were compared qualitatively. The comparison shows a generally good agreement between simulated and observed flood patterns, with some discrepancies mainly attributable to the higher spatial resolution of the hydraulic model compared to satellite-derived flood maps. In fact, small ponds caused by preferential paths of the microtopography were not detected by the satellite derived flood extent.

3.2.1 Strategy of multiple hydrological-hydraulic modelling runs

Considering the very large number of synthetic rainfall hyetographs generated (6 return periods, 5 reference durations, 12 months, a copula sample size of 1000, and 100 temporal cascade profiles per sample, for a total of 36 million of hyetographs), computational efficiency required a strategy for optimizing the hydrological-hydraulic modelling runs. The strategy aimed at achieving a compromise between a representative coverage of the probability spectrum, the variability of reference durations, the uncertainty related to the dependence structure between extreme events at different durations, the variability in rainfall peak distributions, and the computational cost of the hydrologic–hydraulic simulations. Accordingly, four return periods (10, 50, 100, and 200 years) and a subset of representative durations (10, 60, 360 minutes) were selected. For each combination

https://doi.org/10.5194/egusphere-2026-4418
Preprint. Discussion started: 30 July 2026
© Author(s) 2026. CC BY 4.0 License.

of month, return period, and duration, three rainfall profiles corresponding to the minimum, median, and maximum of rainfall depths were retained. This resulted in a total of 432 simulations. The three percentiles corresponding to the span of the hyetographs depths will be labeled as P000, P050 and P100. The simulations were executed using a parallel processing strategy to reduce computational time. Specifically, multiple independent instances of the hydrodynamic model were run concurrently using a multiprocessing framework. The simulations were performed on a workstation equipped with a multi-core CPU (48 logical cores), allocating 6 parallel workers (approximately 8 threads per simulation), which provided a stable compromise between computational efficiency and model performance. The full ensemble of simulations required approximately 16 days of runtime. This computational cost is consistent with the proposed framework and research objectives, supporting decision making for flood-crop damage management and planning and not early warning or emergency management

3.3 Crop types and crop damage curves

The following extensive crop types were selected: rainfed wheat, barley, sunflower and irrigated maize and soybeans. Their choice was driven by both their presence in the study area (Table 1) and the availability of the crop damage curves. Crop spatial distribution was obtained from the European Commission, Joint Research Centre (JRC) (2022), which provides crop-type classification at 10 meters spatial resolution across Europe. Crop phenological timing for the Veneto region was derived from the MIRCA-OS 2025 dataset (Kebede et al., 2025), while the duration of crop growth stages was assigned according to the FAO56 guidelines (Allen et al., 1998). These datasets were combined to reconstruct the spatial and temporal exposure of agricultural areas to flood hazard (see Fig. S17). Annual yields at regional scale were retrieved from the EU27 crop dataset (Tani et al., 2025) for barley, wheat, and sunflowers, from the FAOSTAT (Food and Agriculture Organization of the United Nations, 2025) for Maize (Table 1). Damage curves as a function of duration and flood depth were retrieved from Agenais et al. (2013). Contours of damage curves for the selected crops are reported in Fig. S18. Note that in the initial growth stage, the selected crops are very sensitive to floods even for lower depths and durations, while in the development, mid, and maturity stages, we don't expect significant losses in the case of short duration pluvial floods, since the selected crops are quite resistant to short flood durations. The late stage is more critical for barley and wheat, while soybean and sunflower can be damaged only by significant flood depths.

Table 1. List of selected crops with their relative extent in the study area, the yield and price

Crop	Area (ha)	Area (percent)	Yield (ton/ha)	Price (USD/ton)	rainfed/irrigated
Barley	11.4	0.2	6.4	172	rf
Maize	944.1	16.8	10.5	295.7	ir
Soybeans	704.1	12.6	3.1	282.7	ir
Sunflower	144.6	2.6	3	272.4	rf
Wheat	1238.5	22.1	6	374.2	rf
Total domain	5606.6	100			

https://doi.org/10.5194/egusphere-2026-4418
Preprint. Discussion started: 30 July 2026
© Author(s) 2026. CC BY 4.0 License.

4 Results

The results are presented in three steps. First, we examine how monthly rainfall seasonality propagates into flood extent. Second, we quantify crop-specific expected annual losses by combining the hydraulic outputs with crop exposure and vulnerability. Third, we isolate the role of rainfall duration and intra-event temporal structure by comparing losses across reference durations and hyetograph percentiles.

4.1 Seasonal variability of flood hazard

Rainfall seasonality strongly controls flood extent in the Ceresolo basin. For the same return period, summer events generate substantially larger inundated areas than winter events, with differences reaching approximately 500–600% between the least and most severe months (Fig. 5). This behaviour reflects the seasonal contrast in rainfall extremes: short-duration convective storms in summer produce much larger rainfall depths than winter events at the same return period (Fig. S12).

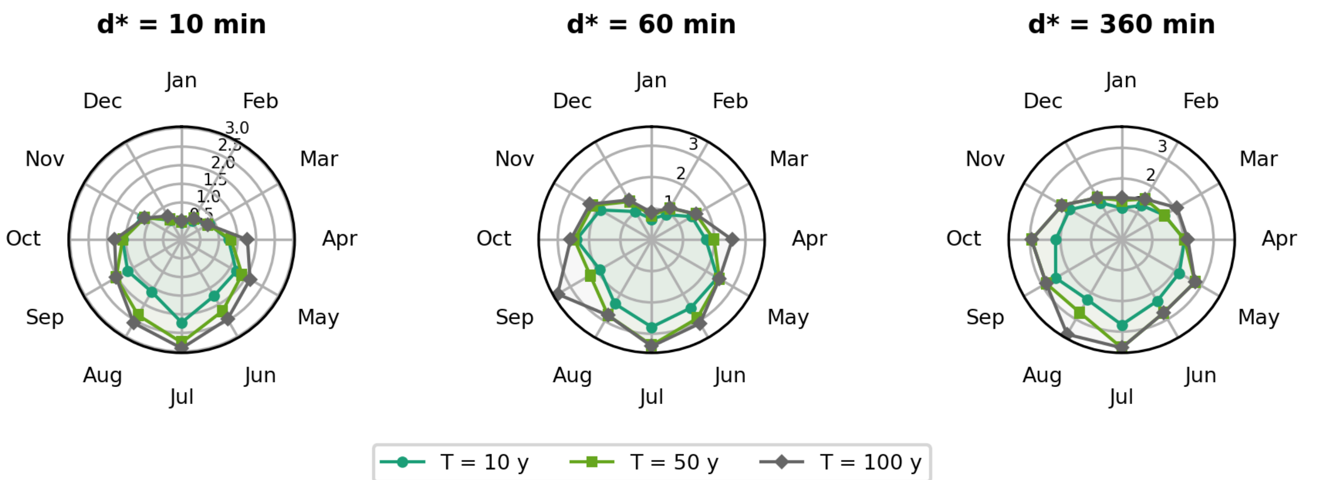

Figure 5. Radar plots of flooded area extent across months for different event durations and return periods (P050 hyetograph percentile). Each spoke represents a month, while radial distance indicates the inundated area ($\times 10^3$ ha) derived from positive flood-depth pixels. Colored lines denote return periods (10-, 50-, and 100-year events), and individual panels correspond to different reference storm durations d* from which the return period has been calculated

4.2 Crop-specific expected annual losses

The crop-specific expected annual loss (EAL) estimates show substantial variability associated with differences in extreme rainfall volume, reference duration, and intra-event temporal structure, as shown in Fig. 6, where results are aggregated by enveloping the different reference durations for each crop and panels are related to each percentile of rainfall depth (P000, P050, P100). The highest EAL values are estimated for irrigated maize and rainfed wheat, but the values may vary by a factor of 10, in the case of Maize, as a result of the variability in the total rainfall depths given by the copula approach. Note that even if the flooded areas of soybeans are more extensive than those of wheat, their EAL values are lower. This is due to the higher resilience of soy plants during the late season (Fig. S18), but also to the longer seasonal exposure of wheat compared with soybean (Fig. S17). Overall, the expected annual losses remain below 1% of total annual crop production, and this is due to the resilience of these crops at low flood durations that are typical of the study area. The main contribution to the total annual economic losses for the selected suite of crops is from wheat and maize. However, the uncertainty of economic losses is particularly high for wheat (Fig 7 and S19).

4.3 Role of rainfall duration and temporal structure

When results are disaggregated considering the different reference durations from which return periods are set (see Fig. S20), the higher the reference duration, the higher the corresponding EAL. This pattern indicates that even if shorter duration rainfall extremes have higher intensity, the impact of flood extent and duration is much lower, because of the importance of the total rainfall volume in the saturation of the soil. It is also worth noting that even if the pluvial flood extent is quite high, especially for the P100 scenario, the expected annual losses are sparsely localized in relatively small areas where flood depths and durations are higher because of terrain depressions (Fig. 8). When flood losses are disaggregated for each month, it is seen that they are mainly concentrated during the initial crop development stages, when these are more vulnerable (Fig. 9), with the exception of barley, for which the main losses occur late in July, when convective storms may be very intense. For the same reason, a significant portion of wheat EAL occurs in the late growth season during the spring/summer months. For all crops with non-negligible expected annual losses, the maximum marginal contribution to the EAL is associated with the 50-year return period events (Fig. 10). This behavior reflects the classical trade-off between event probability and damage severity in risk assessment. While extreme and very rare storms may produce the largest individual damages, events with intermediate return periods dominate the annualized risk because they combine relatively high losses with substantially larger occurrence probabilities.

5 Discussion

The proposed framework highlights the strong sensitivity of agricultural flood-risk estimates to rainfall temporal structure and event duration. In particular, the copula-based modelling of dependence among multiple rainfall durations revealed a substantial uncertainty in expected annual loss estimation, demonstrating that the use of a single representative storm duration may produce significantly biased estimates of flood impacts. This aspect emerged clearly from both the duration-specific analyses and the duration envelope, which showed that different durations may dominate flood losses depending on crop type, season, and hydrological conditions.

One of the main results of the study is that, for the analysed case study, long-duration rainfall events, particularly the 6-hour scenarios, generally produced the highest agricultural losses. This behaviour is mainly associated with longer flood persistence and increased inundation duration, which strongly influence crop damage according to the adopted depth-duration

https://doi.org/10.5194/egusphere-2026-4418
Preprint. Discussion started: 30 July 2026
© Author(s) 2026. CC BY 4.0 License.

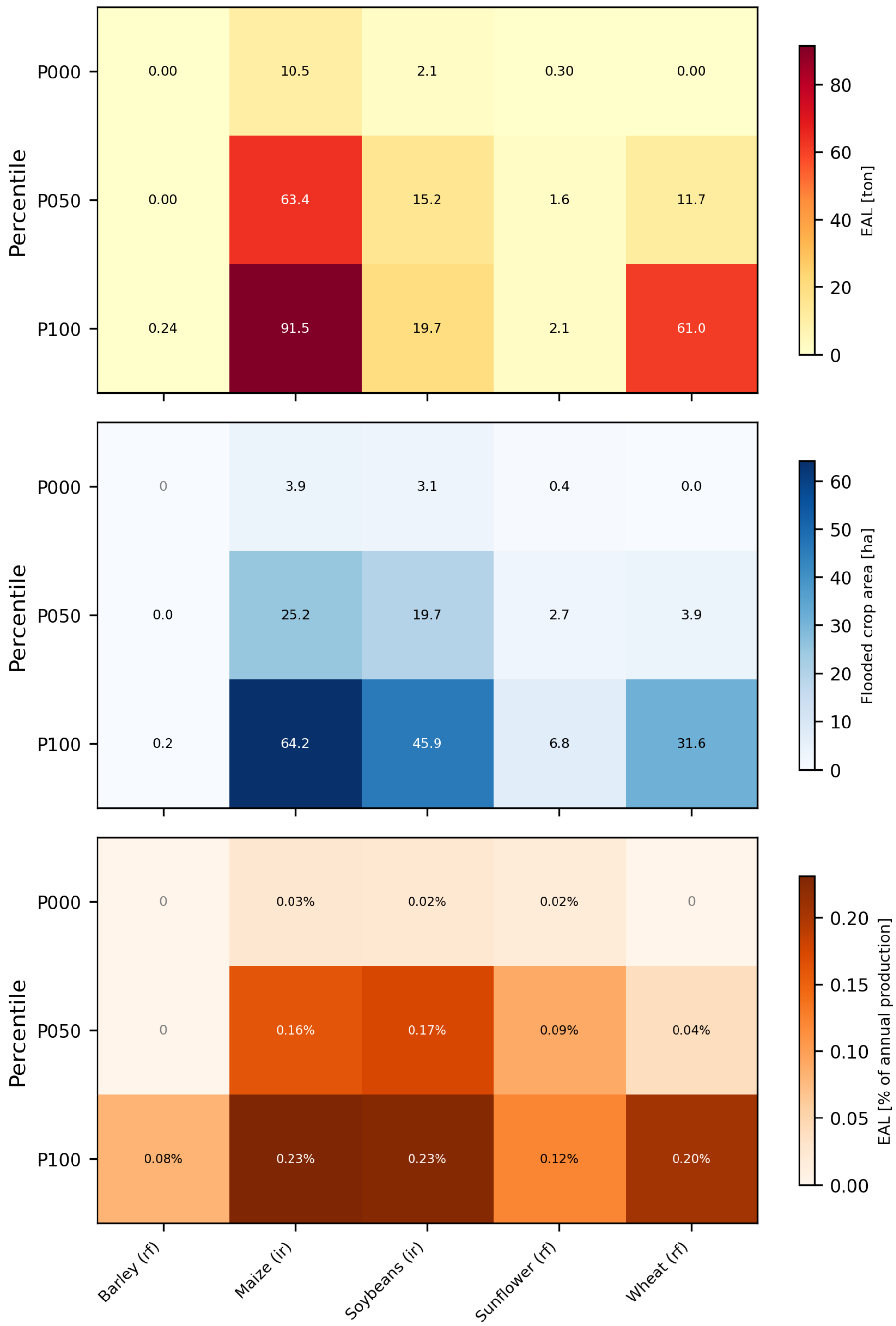

Figure 6. Heatmaps of expected annual loss (EAL), flooded area extent and EAL in percentage with respect to the total annual production across crop types and hyetograph percentiles. Crop losses are expressed in ton, whereas flooded area is reported in hectares. Results represent duration-aggregated envelope conditions

https://doi.org/10.5194/egusphere-2026-4418
Preprint. Discussion started: 30 July 2026
© Author(s) 2026. CC BY 4.0 License.

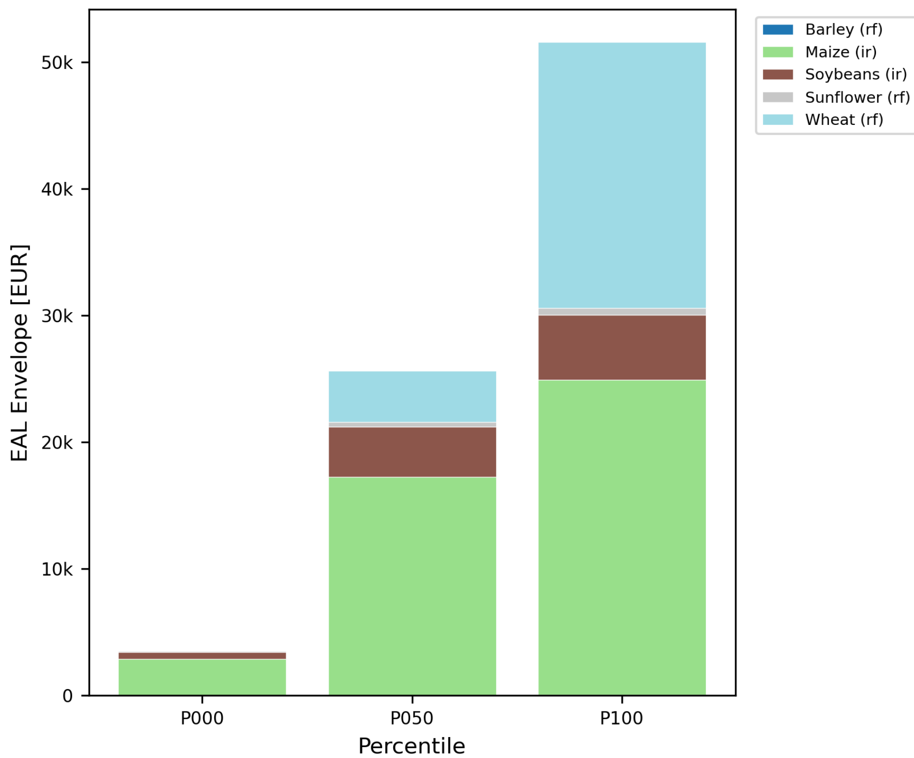

Figure 7. Stacked-bar representation of crop-specific contributions to total expected annual losses (EAL) across hyetograph percentiles. Bar segments indicate the relative importance of individual crop classes in determining overall agricultural flood risk.

vulnerability functions. However, this result should not be interpreted as universally valid. In other hydro-geomorphological settings, such as lowland areas characterized by shallow groundwater tables, poor drainage efficiency, or initially saturated soils, even short-duration convective storms may generate prolonged water stagnation and severe agricultural impacts. Consequently, the relationship between rainfall duration and crop damage remains strongly site-specific.

The approach developed here is able to reproduce complex temporal rainfall structures, including multiple bursts and intermittent precipitation phases, which are commonly observed in real storm events. This characteristic is particularly important for flood-impact assessment because agricultural damage is not controlled exclusively by peak rainfall intensity, but also by antecedent wetness conditions and cumulative soil saturation processes. In this context, a moderate rainfall event occurring over already saturated soils may produce larger impacts than a shorter and more intense storm over dry antecedent conditions. This aspect is also coherent with the adopted event separation criterion, based on a 24-hour dry hiatus. Since consecutive rainfall bursts separated by less than 24 hours are treated as belonging to the same event, the capability of the microcanonical model to reproduce temporally clustered rainfall structures becomes particularly relevant for realistic flood-impact simulation. Such temporal persistence may substantially influence flood duration and, consequently, crop vulnerability. A concrete illustration of

https://doi.org/10.5194/egusphere-2026-4418
Preprint. Discussion started: 30 July 2026
© Author(s) 2026. CC BY 4.0 License.

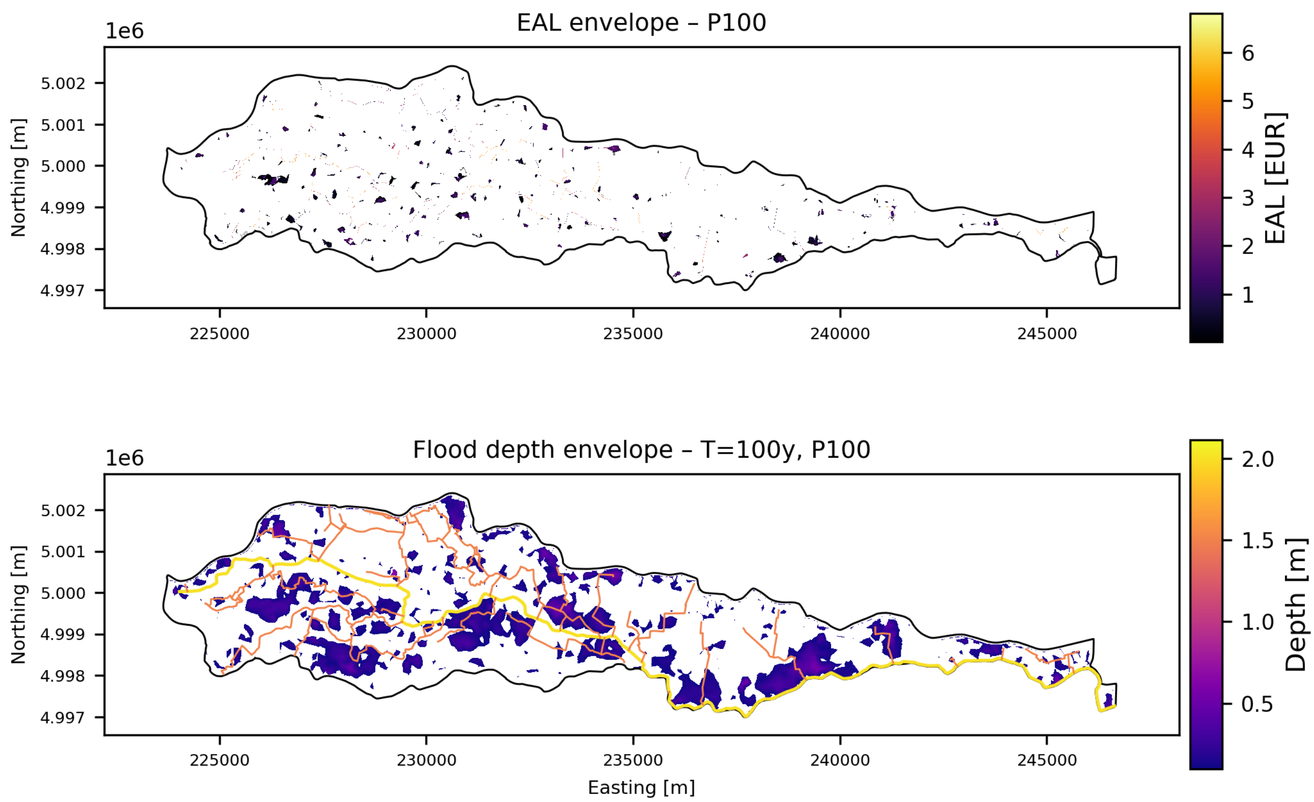

Figure 8. Spatial distribution of duration-envelope expected annual losses (EAL) and flood depths for the 100-year return period under the P100 hyetograph scenario. For each pixel, the duration-envelope EAL is defined as the maximum EAL obtained across all rainfall durations considered. Pixel-level EAL values represent economic damages estimated from the simulated flood depths and crop-specific vulnerability functions.

this mechanism emerges from crop-risk analyses: for the 360 min duration, the expected annual losses of maize and sunflower are nearly identical under the P050 and P100 hyetograph scenarios (Figure S20), despite their different rainfall volumes. This occurs because, for the April events that drive the damage, the lower-volume P050 hyetograph concentrates its peak intensities later in the event, when the soil has already been progressively wetted, whereas the higher-volume P100 is front-loaded (Fig. S21). The resulting surface response, and hence the crop damage, is therefore controlled by the intra-event temporal structure rather than by total volume alone, reinforcing the need to represent event-to-event variability, as done here through the microcanonical model, for a realistic damage estimate.

The results also emphasized the importance of explicitly considering flood duration in agricultural risk assessment. Traditional approaches based exclusively on peak water depth may neglect a critical component of crop vulnerability, especially for crops sensitive to prolonged root anoxia and waterlogging. The implemented depth-duration damage surfaces partially address this limitation by accounting for both inundation intensity and persistence. While extensive cereal crops analysed in this study,

https://doi.org/10.5194/egusphere-2026-4418
Preprint. Discussion started: 30 July 2026
© Author(s) 2026. CC BY 4.0 License.

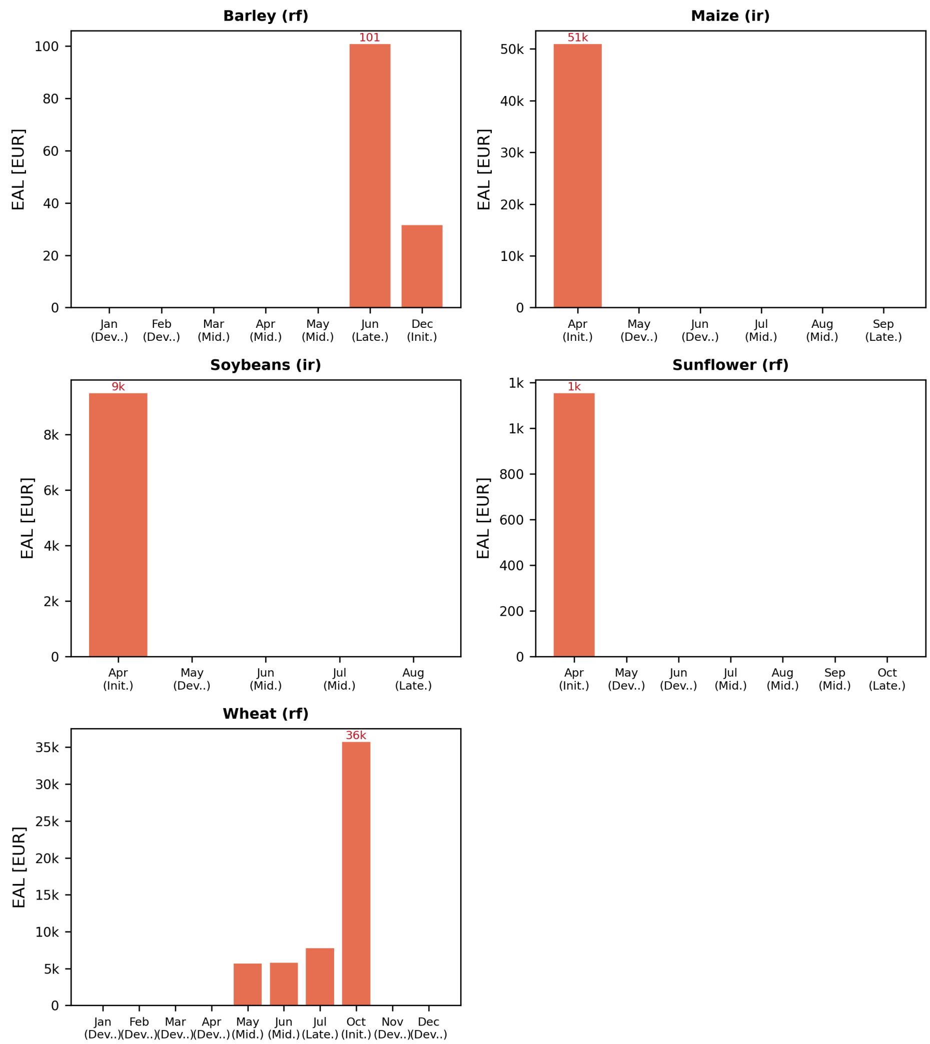

Figure 9. Monthly profile of crop-specific expected annual losses for the P050 hyetograph scenario. Curves represent the duration envelope of economic damages across months, highlighting the seasonal variability of agricultural flood risk in relation to crop phenological stages.

https://doi.org/10.5194/egusphere-2026-4418
Preprint. Discussion started: 30 July 2026
© Author(s) 2026. CC BY 4.0 License.

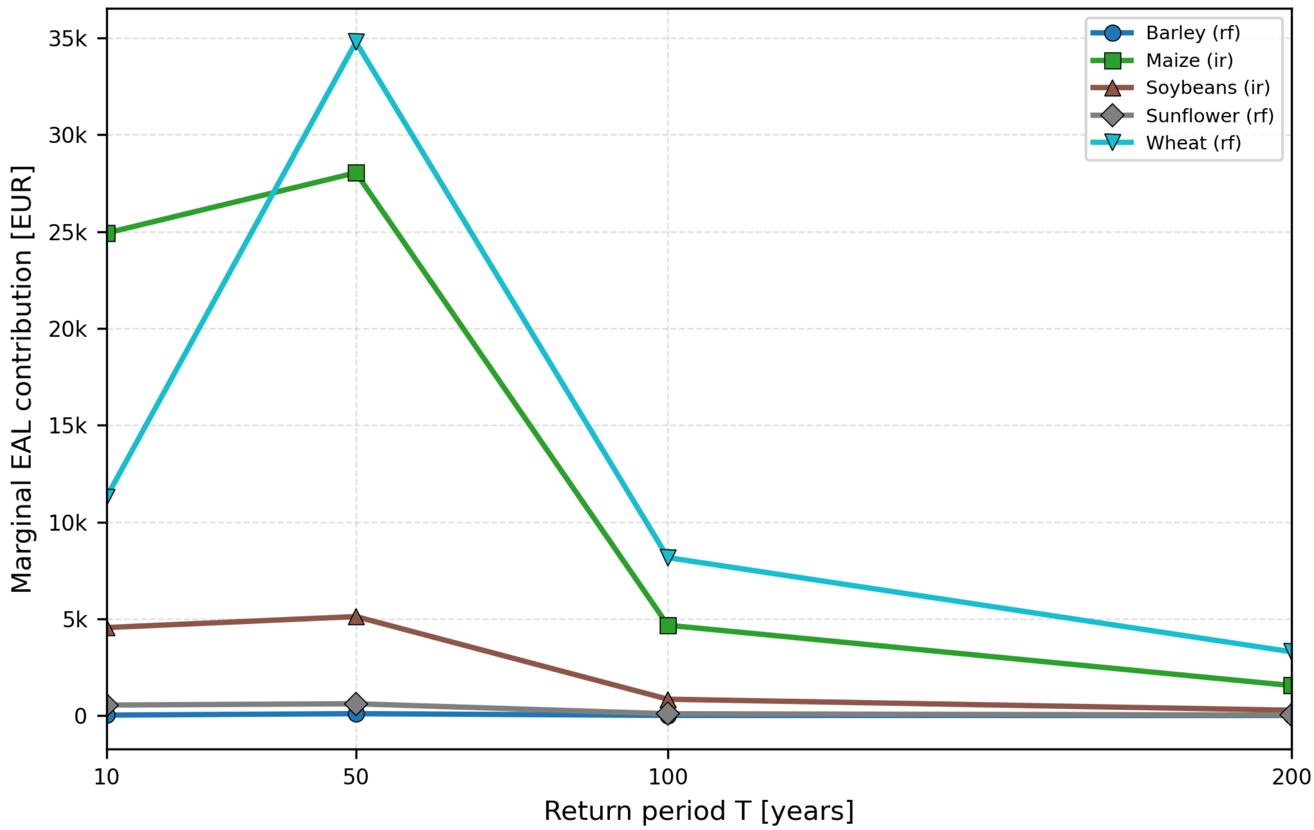

Figure 10. Marginal contribution to total economic losses by each return period for each crop

such as wheat and maize, exhibit relative resilience to short-term inundation, other high-sensitivity categories, particularly horticultural crops and leafy vegetables such as lettuce, spinach, cabbage, and salads, may suffer almost complete production losses even during short flood durations due to rapid root-zone oxygen deprivation and tissue deterioration processes. In fact, according to Agenais et al. (2013), lettuce, such as *Insalata di Lusia PGI* that is grown in the same district of the case study, has a potental damage equal to 100% during all the phenological stages even for few centimeters of submersion.

The present application isolates uncertainty associated with rainfall temporal structure and inter-duration dependence by adopting fixed antecedent hydrological conditions for each scenario. In reality, seasonal variability in soil moisture, groundwater levels, evapotranspiration, irrigation practices, and previous rainfall may substantially affect runoff generation, drainage efficiency, flood extent, and inundation persistence. These effects could be incorporated through ensembles of antecedent conditions derived from continuous hydrological simulations, remote-sensing products, or stochastic soil-moisture models. The framework could therefore be used to distinguish the contribution of rainfall temporal variability from that of hydrological initial conditions.

© Author(s) 2026. CC BY 4.0 License.

The probabilistic rainfall representation adopted in this study relies on a set of simplifying assumptions. In particular, rainfall was assumed to be spatially uniform over the study area, an approximation considered appropriate given the relatively small size of the analysed catchment. In addition, the framework is intentionally formulated for a prescribed statistical characterization of extreme rainfall. This design allows the resulting losses to be interpreted consistently for a given rainfall regime and, more importantly, makes it possible to quantify how losses change when alternative rainfall statistics are imposed. In this sense, the framework is well suited to climate-change applications, since different stationary parameter sets can be used to represent distinct present or future climate conditions and to isolate their effects on flood risk. Where a continuous temporal evolution is of interest, the methodology can also be extended through time-varying marginal distributions and, potentially, non-stationary inter-duration dependence structures informed by convection-permitting climate simulations.

Uncertainty in synthetic rainfall was explicitly addressed through bootstrap resampling, variability in inter-duration dependence, and alternative temporal disaggregation schemes based on the microcanonical model. Additional sources of uncertainty could be incorporated through ensembles of soil-infiltration properties, hydraulic parameters, including roughness coefficients and geometric representations, and alternative topographic datasets. The modular structure of the modelling chain therefore provides a suitable basis for systematic sensitivity analyses and for quantifying the relative contribution of rainfall, hydrological, hydraulic, and topographic uncertainties to the final loss estimates. Previous studies have shown that hydrological forcing uncertainty may dominate hydraulic-parameter uncertainty in flood-inundation modelling (Annis et al., 2020); nevertheless, both contributions can remain substantial. Future applications should therefore propagate these sources jointly along the modelling chain, allowing the framework to serve as a controlled numerical laboratory for identifying the factors that most strongly influence flood extent and economic losses (Apel et al., 2004).

Topographic uncertainty is particularly relevant in agricultural lowlands, where small depressions and local drainage pathways may control water storage and inundation persistence. Because erosion–deposition processes and farming practices can modify microtopography over time, future applications could examine alternative microtopographic configurations or use periodically updated high-resolution elevation data.

The use of damage functions derived from Agenais et al. (2013) represents another limitation. These functions do not fully account for local variability in crop varieties, management practices, soil characteristics, and adaptation strategies, nor for the potential effects of flow velocity and associated mechanical damage. While this simplification may be acceptable in lowland areas dominated by slowly varying inundation processes, it may not be valid in more dynamic flood environments.

The proposed risk framework also adopts a "first-hit" survival approach, where the occurrence of damaging events in earlier months progressively reduces the probability weight associated with subsequent events within the same growing season. While this assumption avoids unrealistically additive seasonal damages, it implicitly neglects the possibility of multiple independent damaging events affecting the same crop during a season. In reality, successive floods may occur and produce cumulative impacts, particularly in highly flood-prone areas. Representing repeated floods would require crop-specific recovery and cumulative-damage functions, which remain poorly established and constitute an important direction for future research. A further assumption embedded in the loss model formulation is the serial independence of damaging-flood occurrence across months, which impacts both the factorisation of the survival probability and the reduction of the conditional expected loss to its

https://doi.org/10.5194/egusphere-2026-4418
Preprint. Discussion started: 30 July 2026
© Author(s) 2026. CC BY 4.0 License.

unconditional counterpart. In reality, flood occurrence exhibits temporal clustering, driven by persistent seasonal-to-interannual climate states and by catchment wetness memory, the latter being closely related to the antecedent-moisture limitation discussed above. Flood-rich and flood-poor periods have been documented across Europe (Merz et al., 2016; Lun et al., 2020), and teleconnection patterns such as the North Atlantic Oscillation modulate winter precipitation, flood occurrence, and associated losses in the Euro-Mediterranean region (Trigo et al., 2004; Marani and Zanetti, 2015; Zanardo et al., 2019). It is worth noting, however, that such clustering has a limited and predictable effect on the proposed formulation. The leading-order contribution to the expected annual loss depends only on the marginal monthly probabilities $p_{m,i}$, while inter-month dependence enters exclusively through the first-hit correction terms, which involve the joint occurrence of two damaging events within the same season and are therefore of second order in the monthly occurrence probabilities. Moreover, under the positive dependence indicated by the literature, the probability of a damaging flood conditional on the absence of previous damaging floods is lower than its unconditional value, so the independence assumption slightly overestimates the expected annual loss, i.e., it is conservative for risk-assessment purposes. A fully conditional formulation would require expressing the monthly hazard marginals as functions of a seasonal climate state, e.g., through covariate-dependent non-asymptotic extreme-value models or by exploiting the year-specific parameter variability of the full MEVD (Marani and Ignaccolo, 2015), at the cost of multiplying the entire hazard-to-damage simulation chain by the number of climate states considered and of the introduction of parametric assumptions and the associated additional parameters.

Overall, the framework should be regarded as a modular platform rather than as a fixed modelling configuration. Its components can be progressively expanded to examine alternative rainfall climates, spatial rainfall patterns, antecedent hydrological states, hydraulic and topographic uncertainty, locally calibrated crop vulnerability, and repeated-impact and recovery processes. This flexibility makes the methodology suitable not only for estimating agricultural flood risk, but also for identifying which components of the hazard–damage chain most strongly control flood extent, persistence, and economic losses.

6 Conclusions

This study developed a probabilistic framework for agricultural flood-risk assessment that integrates multi-duration rainfall frequency analysis, copula-based inter-duration dependence, stochastic temporal disaggregation, hydraulic modelling, and crop-specific depth-duration vulnerability functions. Its main contribution is the explicit propagation of rainfall duration and temporal-structure variability from design-event generation to spatially distributed agricultural losses.

The results show that agricultural flood risk cannot be robustly represented using a single rainfall duration or a single deterministic design hyetograph. Different storm durations may dominate the losses of different crops and seasons, while their effects also depend on local hydrological and geomorphological conditions. In the analysed case study, longer duration events generally generated the largest losses because of prolonged inundation and waterlogging; however, the framework demonstrates that the critical duration is an outcome of the coupled rainfall–flood–damage system rather than a fixed property of the study area. By preserving the statistical dependence among rainfall depths at different durations, the proposed approach also avoids the unrealistic assumption that all within-storm durations simultaneously correspond to the same return period. The

© Author(s) 2026. CC BY 4.0 License.

stochastic disaggregation procedure further enables the representation of multi-burst and temporally clustered rainfall events, which are particularly relevant for soil saturation, flood persistence, and crop vulnerability. The framework is intentionally formulated for a prescribed rainfall regime, allowing losses to be compared consistently across alternative present or future rainfall statistics. Its modular structure also enables additional sources of uncertainty, including antecedent soil moisture, spatial rainfall variability, infiltration properties, hydraulic parameters, and topographic information, to be incorporated through ensemble experiments. It can therefore support not only agricultural flood-risk estimation, but also sensitivity analysis, climate-change assessment, and the identification of the processes that most strongly control flood losses. Overall, the proposed methodology provides a flexible and transferable basis for evaluating agricultural flood risk while explicitly accounting for rainfall seasonality, duration, temporal structure, and crop-specific vulnerability. These capabilities may support the design of climate-adaptation strategies, agricultural flood-management measures, and more robust risk-informed planning in flood-prone rural areas.

Code and data availability. Figures S1-S21 and Tables S1-S3 are available in the Supplement. The Python framework implementing the methodology (StormGenerator, HecRasRainBuilder, HecRasBatchLauncher, and CropRiskCalculator modules) is openly available on Zenodo (Annis et al., 2026), released under the MIT License, and developed on GitHub at https://github.com/antonioannis/flood-risk-agriculture. The SMEV routines were adapted from the MATLAB code of Marra (2020), and the vine-copula and micro-canonical cascade routines from the MATLAB code of Cache (2025), both released under CC-BY 4.0. Rainfall data were provided by the Veneto Environmental Protection Agency (*ARPAV*). The surveyed cross sections were provided by the Consorzio Adige Po. The regional DTM is available online at https://idt2.regione.veneto.it/idt/downloader/download (last access on 09/05/2026) Crop spatial distribution was obtained from the European Commission, Joint Research Centre (JRC) (2022). Crop phenological timing for the Veneto region was derived from the MIRCA-OS 2025 dataset (Kebede et al., 2025), while the duration of crop growth stages was obtained from the FAO56 guidelines (Allen et al., 1998). Regional annual yields for barley, wheat, and sunflower were retrieved from the EU27 crop dataset (Tani et al., 2025), whereas maize yields were obtained from FAOSTAT (Food and Agriculture Organization of the United Nations, 2025).

Author contributions. AA: conceptualization, methodology, software, formal analysis, investigation, data curation, visualization, and writing (original draft preparation). FN: conceptualization, supervision, and writing (review and editing). MM: conceptualization, supervision, and writing (review and editing).

Competing interests. The authors declare there are no conflicts of interest for this manuscript.

Acknowledgements. This study was carried out within the RETURN Extended Partnership and received funding from the European Union Next-GenerationEU (National Recovery and Resilience Plan—NRRP, Mission 4, Component 2, Investment 1.3—D.D. 1243 2/8/2022,

https://doi.org/10.5194/egusphere-2026-4418
Preprint. Discussion started: 30 July 2026
© Author(s) 2026. CC BY 4.0 License.

PE0000005). AA was supported by Fondazione Cassa di Risparmio di Padova e Rovigo. We thank Francesco Marra and Tabea Cache and co-authors for making the code of their SMEV and design-storm-generation models, respectively, openly available, which supported the development of the stochastic rainfall generation modules of this work.

© Author(s) 2026. CC BY 4.0 License.

References

Agenais, A., Grelot, F., Bremond, P., and Erdlenbruch, K.: Dommages des inondations au secteur agricole: guide méthodologique et fonctions nationales, Ph.D. thesis, irstea, 2013.

Allen, R. G., Pereira, L. S., Raes, D., Smith, M., et al.: FAO Irrigation and drainage paper No. 56, Rome: food and agriculture organization of the United Nations, 56, e156, 1998.

Andria, S., Borga, M., and Marani, M.: Thermodynamic versus large-scale controls on extreme precipitation: Temporal scale dependence and Clausius-Clapeyron scaling redefined, Geophysical Research Letters, 52, e2025GL115 204, 2025.

Annis, A., Nardi, F., Volpi, E., and Fiori, A.: Quantifying the relative impact of hydrological and hydraulic modelling parameterizations on uncertainty of inundation maps, Hydrological Sciences Journal, 65, 507–523, 2020.

Annis, A., Nardi, F., and Marani, M.: Agricultural flood risk under seasonally varying rainfall extremes and crop vulnerability, Zenodo [code], Zenodo [code], https://doi.org/10.5281/zenodo.21475252, 2026.

Apel, H., Thieken, A. H., Merz, B., and Blöschl, G.: Flood risk assessment and associated uncertainty, Natural Hazards and Earth System Sciences, 4, 295–308, 2004.

Bremond, P., Grelot, F., and Agenais, A.-L.: Economic evaluation of flood damage to agriculture–review and analysis of existing methods, Natural Hazards and Earth System Sciences, 13, 2493–2512, 2013.

Cache, T.: Realistic design storm model, Zenodo [code], Zenodo [code], https://doi.org/10.5281/zenodo.15119797, 2025.

Cache, T., Bevacqua, E., Zscheischler, J., Müller-Thomy, H., and Peleg, N.: Simulating realistic design storms: A joint return period approach, Water Resources Research, 61, e2024WR039 739, 2025.

Clement, M. A., Kilsby, C. G., and Moore, P.: Multi-temporal synthetic aperture radar flood mapping using change detection, Journal of Flood Risk Management, 11, 152–168, 2018.

Devò, P., Caruso, M. F., Borga, M., and Marani, M.: Estimates of rare rainfall extremes in ungauged areas, Geophysical Research Letters, 52, e2024GL113 576, 2025.

European Commission, Joint Research Centre (JRC): EUCROPMAP 2022, https://doi.org/10.2905/555e5d1d-1aae-4320-a716-2e6d18aa1e7c, dataset, 2022.

Fitzgerald, D.: Analysis of extreme rainfall using the log logistic distribution, Stochastic Environmental Research and Risk Assessment, 19, 249–257, 2005.

Food and Agriculture Organization of the United Nations: FAOSTAT Statistical Database, https://www.fao.org/faostat/, accessed: 2026-01-15, 2025.

Griffis, V. and Stedinger, J.: Log-Pearson type 3 distribution and its application in flood frequency analysis. I: Distribution characteristics, Journal of Hydrologic Engineering, 12, 482–491, 2007.

Hosking, J. R. and Wallis, J. R.: Regional frequency analysis, New York, 1997.

Kebede, E. A., Oluoch, K. O., Siebert, S., Mehta, P., Hartman, S., Jägermeyr, J., Ray, D., Ali, T., Brauman, K. A., Deng, Q., et al.: A global open-source dataset of monthly irrigated and rainfed cropped areas (MIRCA-OS) for the 21st century, Scientific Data, 12, 208, 2025.

Lisniak, D., Franke, J., and Bernhofer, C.: Circulation pattern based parameterization of a multiplicative random cascade for disaggregation of observed and projected daily rainfall time series, Hydrology and Earth System Sciences, 17, 2487–2500, 2013.

Lucaora, T., Annis, A., Nardi, F., Rulli, M. C., and Chiarelli, D. D.: Distributed hydrodynamic modelling for assessing flood impacts on crops: Assessing flood-resilient crop management in a coastal basin of central Italy, Agricultural Water Management, 309, 109 352, 2025.

https://doi.org/10.5194/egusphere-2026-4418
Preprint. Discussion started: 30 July 2026
© Author(s) 2026. CC BY 4.0 License.

Lun, D., Fischer, S., Viglione, A., and Blöschl, G.: Detecting flood-rich and flood-poor periods in annual peak discharges across Europe, Water Resources Research, 56, e2019WR026 575, 2020.

Marani, M. and Ignaccolo, M.: A metastatistical approach to rainfall extremes, Advances in Water Resources, 79, 121–126, 2015.

Marani, M. and Zanetti, S.: Long-term oscillations in rainfall extremes in a 268 year daily time series, Water Resources Research, 51, 639–647, 2015.

Marra, F.: A unified framework for extreme sub-daily precipitation frequency analyses based on ordinary events – data & codes, Zenodo [code], Zenodo [code], https://doi.org/10.5281/zenodo.3971558, 2020.

Marra, F., Zoccatelli, D., Armon, M., and Morin, E.: A simplified MEV formulation to model extremes emerging from multiple nonstationary underlying processes, Advances in Water Resources, 127, 280–290, 2019.

Marra, F., Borga, M., and Morin, E.: A unified framework for extreme subdaily precipitation frequency analyses based on ordinary events, Geophysical Research Letters, 47, e2020GL090 209, 2020.

Massey, F. J.: The Kolmogorov-Smirnov test for goodness of fit, Journal of the American Statistical Association, 46, 68–78, https://doi.org/10.1080/01621459.1951.10500769, 1951.

Merz, B., Nguyen, V. D., and Vorogushyn, S.: Temporal clustering of floods in Germany: Do flood-rich and flood-poor periods exist?, Journal of Hydrology, 541, 824–838, 2016.

Müller, H. and Haberlandt, U.: Temporal rainfall disaggregation using a multiplicative cascade model for spatial application in urban hydrology, Journal of Hydrology, 556, 847–864, 2018.

Müller-Thomy, H.: Temporal rainfall disaggregation using a micro-canonical cascade model: possibilities to improve the autocorrelation, Hydrology and Earth System Sciences, 24, 169–188, 2020.

Olsson, J.: Evaluation of a scaling cascade model for temporal rain-fall disaggregation, Hydrology and earth system sciences, 2, 19–30, 1998.

Papalexiou, S. M. and Koutsoyiannis, D.: A global survey on the seasonal variation of the marginal distribution of daily precipitation, Advances in Water Resources, 94, 131–145, 2016.

Scorzini, A. R., Di Bacco, M., and Manella, G.: Regional flood risk analysis for agricultural crops: Insights from the implementation of AGRIDE-c in central Italy, International Journal of Disaster Risk Reduction, 53, 101 999, 2021.

Scorzini, A. R., Paz Idarraga, C. D., and Molinari, D.: An integrated regionalization framework for incorporating flood seasonality into agricultural flood risk assessments, Stochastic Environmental Research and Risk Assessment, 40, 21, 2026.

Sharda, V., Das, P., and Ojasvi, P.: Probability distribution of extreme rainfall series for conservation planning in a sub-humid climate, Applied Engineering in Agriculture, 24, 447–453, 2008.

Shrestha, B. B., Okazumi, T., Miyamoto, M., and Sawano, H.: Flood damage assessment in the P ampanga river basin of the P hilippines, Journal of Flood Risk Management, 9, 355–369, 2016.

Shrestha, B. B., Perera, E. D. P., Kudo, S., Miyamoto, M., Yamazaki, Y., Kuribayashi, D., Sawano, H., Sayama, T., Magome, J., Hasegawa, A., et al.: Assessing flood disaster impacts in agriculture under climate change in the river basins of Southeast Asia, Natural Hazards, 97, 157–192, 2019.

Shrestha, B. B., Kawasaki, A., and Zin, W. W.: Development of flood damage functions for agricultural crops and their applicability in regions of Asia, Journal of Hydrology: Regional Studies, 36, 100 872, 2021.

Tani, A. C., Pulighe, G., Gabrieli, G., Cardillo, C., and Lupia, F.: Comprehensive Collection of EU-27 crops statistics: a harmonized regional dataset of area and production, Scientific Data, 12, 1076, 2025.

https://doi.org/10.5194/egusphere-2026-4418
Preprint. Discussion started: 30 July 2026
© Author(s) 2026. CC BY 4.0 License.

Trigo, R. M., Pozo-Vázquez, D., Osborn, T. J., Castro-Díez, Y., Gámiz-Fortis, S., and Esteban-Parra, M. J.: North Atlantic Oscillation influence on precipitation, river flow and water resources in the Iberian Peninsula, International Journal of Climatology, 24, 925–944, 2004.

Wilson, P. and Toumi, R.: A fundamental probability distribution for heavy rainfall, Geophysical Research Letters, 32, 2005.

Zanardo, S., Nicotina, L., Hilberts, A. G., and Jewson, S. P.: Modulation of economic losses from European floods by the North Atlantic Oscillation, Geophysical Research Letters, 46, 2563–2572, 2019.

Zorzetto, E., Botter, G., and Marani, M.: On the emergence of rainfall extremes from ordinary events, Geophysical Research Letters, 43, 8076–8082, 2016.